Retinoic acid signaling balances adult distal lung epithelial progenitor cell growth and differentiation

John-Poul Ng-Blichfeldt [a,b,*,1], Anneke Schrik [a], Rosa K. Kortekaas [a], Jacobien A. Noordhoek [c], Irene H. Heijink [c], Pieter S. Hiemstra [d], Jan Stolk [d], Melanie Königshoff [b,e], Reinoud Gosens [a,*]

[a] Department of Molecular Pharmacology, Groningen Research Institute for Asthma and COPD (GRIAC), University of Groningen, Groningen 9713AV, The Netherlands
[b] Lung Repair and Regeneration Unit, Helmholtz-Zentrum Munich, Ludwig-Maximilians-University, University Hospital Grosshadern, Member of the German Center of Lung Research (DZL), Munich 81377, Germany
[c] University of Groningen, University Medical Center Groningen, Department of Pathology and Medical Biology and Pulmonology, Groningen Research Institute for Asthma and COPD (GRIAC), Groningen, 9713GZ, The Netherlands
[d] Department of Pulmonology, Leiden University Medical Center, Leiden 2333ZA, The Netherlands
[e] Division of Pulmonary Sciences and Critical Care Medicine, School of Medicine, University of Colorado, Aurora, CO 80045, USA.

ARTICLE INFO

ABSTRACT

Background: Despite compelling data describing pro-regenerative effects of all-trans retinoic acid (ATRA) in pre-clinical models of chronic obstructive pulmonary disease (COPD), clinical trials using retinoids for emphysema patients have failed. Crucial information about the specific role of RA signaling in adult rodent and human lung epithelial progenitor cells is largely missing.
Methods: Adult lung organoid cultures were generated from isolated primary mouse and human lung epithelial cells, and incubated with pharmacological pathway modulators and recombinant proteins. Organoid number and size were measured, and differentiation was assessed with quantitative immunofluorescence and gene expression analyses.
Findings: We unexpectedly found that ATRA decreased lung organoid size, whereas RA pathway inhibition increased mouse and human lung organoid size. RA pathway inhibition stimulated mouse lung epithelial proliferation *via* YAP pathway activation and epithelial-mesenchymal FGF signaling, while concomitantly suppressing alveolar and airway differentiation. HDAC inhibition rescued differentiation in growth-augmented lung organoids.
Interpretation: In contrast to prevailing notions, our study suggests that regenerative pharmacology using transient RA pathway inhibition followed by HDAC inhibition might hold promise to promote lung epithelial regeneration in diseased adult lung tissue.
Fund: This project is funded by the Lung Foundation Netherlands (Longfonds) grant 6.1.14.009 (RG, MK, JS, PSH) and W2/W3 Professorship Award by the Helmholtz Association, Berlin, Germany (MK).

1. Introduction

Endogenous lung regeneration is overwhelmed in chronic obstructive pulmonary disease (COPD), a widely prevalent syndrome clinically defined by airflow obstruction and progressive lung function decline [1]. Pathologically, COPD is characterized by bronchitis, small airways disease, and destruction both of the smallest airways and of gas-exchanging alveolar tissue (emphysema); these features stem from a chronic inflammatory state due to long-term exposure to airborne pollutants including cigarette smoke. Currently, there are no disease-modifying treatments able to halt or reverse structural defects associated with COPD [1,2]. Novel pharmacological therapies to bolster endogenous regenerative mechanisms are desperately needed to improve patient quality of life and to ease the global healthcare burden. The adult mammalian lung contains progenitor cell populations including basal cells and secretory club cells in the airways, rare putative multipotent stem cells in the distal airways, and alveolar type 2 (AT2) cells within alveoli [3]; these populations can maintain and repair mild damage, and to a limited extent, regenerate severe lung injury

* Corresponding authors at: Department of Molecular Pharmacology, Groningen Research Institute for Asthma and COPD (GRIAC), University of Groningen, Groningen 9713AV, The Netherlands.
E-mail addresses: jpblich@mrc-lmb.cam.ac.uk (J.-P. Ng-Blichfeldt), r.gosens@rug.nl (R. Gosens).
[1] Current address: MRC Laboratory of Molecular Biology, Cambridge Biomedical Campus, Francis Crick Avenue, Cambridge CB2 0QH, UK

Research in context

Evidence before this study

Administration of retinoic acid promoted lung regeneration in rodent models of adult chronic lung disease, yet clinical trials with retinoids in COPD patients failed. The impact of RA pathway modulation on adult lung epithelial stem cell function has been little explored.

Added value of this study

In this study we demonstrate that RA restricts adult lung organoid growth, whereas RA pathway inhibition promoted lung epithelial proliferation while suppressing differentiation. Moreover, HDAC inhibition restored differentiation in growth-enhanced lung epithelium. Our study thus sheds light on the role of RA signaling in adult lung epithelial progenitor function.

Implications of all the available evidence

In contrast to prevailing ideas, our data suggest transient RA pathway inhibition followed by HDAC inhibition may offer therapeutic benefit for COPD patients.

[4–12]. Pharmacologically targeting these progenitor populations may hold promise as a novel therapeutic strategy to augment lung regeneration in COPD.

The retinoic acid (RA) signaling pathway has emerged as a promising target for therapeutic regenerative pharmacology in adult chronic lung diseases [13]. RA is derived from dietary vitamin A, which circulates as retinol prior to entering target cells, where it is oxidized to all-trans RA (ATRA) by retinol- and retinaldehyde- dehydrogenases (RALDHs). ATRA is transcriptionally active *via* interactions with heterodimers of RA receptors (RAR-α, −β, or −γ) and retinoid X receptors (RXR-α, −β, or −γ) that bind to RA response elements (RAREs) in regulatory regions of target genes [14]. Studies in mice revealed that RA is a critical regulator of both embryonic lung development and post-natal alveolarization [15–19]. *In vitro*, ATRA stimulated human lung microvascular angiogenesis [20] and induced lung fibroblast elastin synthesis [21]. In man, epidemiological evidence revealed associations between vitamin A deficiency and reduced lung function in children that was alleviated by maternal vitamin A supplementation [22]. RARβ variants are associated with reduced adult lung function [23]. Moreover, RA pathway perturbations correlated with emphysematous lung destruction [20], and cultured lung fibroblasts isolated from emphysema patients exhibited impaired RA-induced elastin synthesis compared to non-diseased control fibroblasts [24], suggesting defective retinoid-driven regeneration may contribute to COPD. Numerous pre-clinical studies using *in vivo* rodent models of COPD/emphysema revealed the striking ability of ATRA to induce structural remodeling consistent with alveolar regeneration [25–32], however, the few clinical trials exploring RA or retinoid analogues in patients with emphysema failed to meet primary clinical endpoints [33–36]. Interpretation of these findings is hampered by a poor understanding about the specific role of RA signaling in adult lung epithelial progenitor cell function.

We addressed this knowledge gap using an adult lung organoid model, which recapitulates critical processes during lung regeneration [37]. Unexpectedly, we found that RA pathway stimulation decreased lung organoid size and inhibited lung epithelial proliferation. In contrast, RA pathway inhibition promoted epithelial proliferation in mouse lung organoids and in organoids derived from lung tissue from COPD patients. In mouse lung organoids, augmented proliferation induced by RA inhibition occurred with a concomitant suppression of

airway and alveolar epithelial differentiation, and was mediated by yes-associated protein (YAP) pathway activation and fibroblast-epithelial fibroblast growth factor (FGF) signaling. Histone deacetylase (HDAC) inhibition combined with ATRA was identified as a potential strategy to restore differentiation in adult lung epithelial cells.

2. Materials and methods

2.1. Reagents

Pharmacological agents used: All-trans retinoic acid ([ATRA] Sigma Aldrich, Poole, UK #R2625), BMS493 (Tocris, Bristol, UK #3509), CH5183284 (Selleck Chem, Munich, Germany #S7665), Verteporfin (Sigma #SML0534, kindly provided by Dr. Ruud Bank, UMCG), SAHA (Tocris #4652). Pharmacological agents were stored as stock solution in dimethyl sulfoxide (DMSO) at -20 °C. Prior to treatment, agents were further diluted in DMSO so that the volume added to culture was equal across treatment groups. Equal volumes of DMSO were added for vehicle control. Recombinant proteins used: FGF7 (R&D Systems, Abingdon, UK #251-KG), FGF10 (R&D Systems #345-KG). Recombinant proteins were reconstituted in sterile filtered PBS with 0·1% (*w/v*) BSA and stored at -20 °C.

2.2. Ethics

All animal experiments were performed according to the Ethics Committee guidelines of the University of Groningen. Human lung tissue specimens were obtained with full informed consent from patients undergoing lung volume reduction surgery or lung transplantation at University of Medical Center Groningen (UMCG). The study protocol was consistent with the Research Code of the University Medical Center Groningen (https://www.umcg.nl/EN/Research/Researchers/General/ResearchCode) and national ethical and professional guidelines ("Code of conduct; Dutch federation of biomedical scientific societies", htttp://www.federa.org). All tissue samples were anonymized prior to use.

2.3. Cell culture

Mlg mouse lung fibroblasts ([MLg2908, CCL206], ATCC, Wesel, Germany) were maintained in DMEM/F12 medium (Life technologies, Carlsbad, USA) supplemented with 10% fetal bovine serum (FBS, PAA Laboratories, Pasching, Austria), penicillin/streptomycin (100 U/ml), glutamine (1%, Life Technologies #35050–061) and Amphotericin B (1×, Gibco). MRC5 human lung fibroblasts (ATCC #CCL-171) were maintained in F12 medium supplemented with 10% FBS, penicillin/streptomycin (100 U/ml), glutamine (1%) and Amphotericin B (1×). Cells were maintained at 37 °C in a humidified incubator with 5% CO_2. Prior to organoid culture, Mlg or MRC5 cells at 90% confluence were proliferation-inactivated in medium containing mitomycin C (10 μg/ml, Sigma #M4287) for 2 h, followed by 3 washes in warm PBS (Life technologies) and trypsinization.

2.4. Lung epithelial cell isolation

Epithelial cells were isolated from adult mouse lung with antibody-conjugated magnetic beads (microbeads) as previously described [38,39]. Pathogen-free wild type C57BL/6 N mice (minimum 8 weeks old) were anaesthetized and sacrificed, lungs were flushed with PBS and instilled with low-melt agarose (Sigma #A9414) and dispase (BD Biosciences, Oxford, UK #354235) and incubated at room temperature for 45 min. Trachea and extrapulmonary airways were removed, and remaining lobes were homogenized to single-cell suspension in DMEM containing DNase1 (Applichem, Germany #A3778). Suspension was passed through nylon filters and incubated with CD45 (Miltenyi Biotec, Teterow, Germany #130–052-301) and CD31 (Miltenyi, #130–097-418) microbeads, and then passed through LS columns (Miltenyi

#130–091-051). The CD31$^-$/CD45$^-$ flow-through was incubated with EpCAM (CD326) microbeads (Miltenyi #130–105-958) for epithelial cell positive selection with LS columns. Mouse lung EpCAM$^+$ cells were resuspended in DMEM with 10% FBS, and seeded into Matrigel immediately after isolation with equivalent numbers of Mlg cells as described in the next section. Human lung epithelial cells were isolated from lung tissue specimens obtained from 3 GOLD stage IV COPD patients undergoing lung transplantation, and 1 GOLD stage II COPD patient undergoing lung tumor resection (patient characteristics in Table S1). Peripheral lung tissue was homogenized overnight at 4 °C in EDTA (Gibco) containing 0·25% trypsin, penicillin/streptomycin (100 U/ml), Collagenase A (2 mg/ml, Roche) and DNase I (0·04 mg/ml, Sigma). The resulting suspension was filtered prior to incubation with EpCAM microbeads (Miltenyi #130–061-101) and positive selection with LS columns. Human EpCAM$^+$ cells were seeded into the Matrigel assay immediately after isolation with equivalent numbers of MRC5 cells.

2.5. Lung organoid culture

The lung organoid (spheroid) assay is based on published protocols with slight modifications [5,40,41]. Equivalent numbers of EpCAM$^+$ cells and fibroblasts were seeded per insert in 100 μl growth factor-reduced Matrigel (Fisher Scientific, Landsmeer, The Netherlands #11523550) diluted 1:1 with DMEM/F12 containing 10% FBS into transwell inserts for 24-well plates (Thermo Fischer Scientific, Waltham, USA 10421761). For mouse lung organoid cultures, 20,000 mouse lung EpCAM$^+$ cells were seeded with 20,000 Mlg cells; for human lung organoid cultures, 3500–30,000 human lung EpCAM$^+$ cells were seeded with 3500–30,000 MRC5 cells. Mouse lung organoid cultures were maintained in DMEM/F12 containing 5% FBS, penicillin/streptomycin (100 U/ml), glutamine (1%), Amphotericin B (1×), insulin-transferrin selenium (1×, Gibco #15290018), recombinant mouse EGF (0·025 μg/ml, Sigma #SRP3196), Cholera toxin (0·1 μg/ml, Sigma #C8052) and bovine pituitary extract (30 μg/ml, Sigma #P1476). ATRA was freshly added to organoid culture media (0·01 μM, Sigma #R2625) for all experiments except for those investigating effects of ATRA, in which ATRA was added at the indicated concentrations. Y-27632 (10 μM, Tocris #1254) was added for the first 48 h of culture. Human lung organoids were maintained in SAGM (Promocell #C21170) supplemented with 1% FBS, with the indicated ATRA or RA inhibitor treatments. All organoid cultures were maintained at 37 °C in a humidified incubator with 5% CO$_2$. Medium was refreshed every 2–3 days.

2.6. Quantification of organoid number, size and differentiation

To quantify organoid colony forming efficiency, total number of organoids per well was manually counted 7 days after seeding using a light microscope at 10× magnification. Data points represent the mean of 2 wells per condition per independent experiment. Organoid diameter was measured 14 days after seeding for mouse cultures, and 21 days after seeding for human cultures, with a light microscope connected to NIS-Elements software (Nikon). All organoids within >3 random fields of view were measured per well; 2 wells were analyzed per condition per independent experiment. Human lung organoids were defined as >50 μm diameter. To quantify SFTPC$^+$ or ACT$^+$ spheroids, immunofluorescence-stained day 14 organoid cultures were manually analyzed for expression using a fluorescence microscope at 40× magnification. >150 organoids were analyzed per condition per independent experiment.

2.7. Immunofluorescence

Organoid cultures were washed once with PBS, fixed with ice-cold acetone/methanol (1:1) for 12 min at -20 °C, washed again with PBS and blocked in PBS with 5% (w/v) BSA. Whole-mount immunofluorescence was performed with antibodies diluted in PBS with 0·1% (w/v) BSA and 0·1% Triton-X100. Cultures were incubated with primary antibodies at 4 °C overnight, washed 3× in PBS for 15 min each, and incubated with secondary antibodies at 4 °C overnight. Cultures were excised and mounted on glass slides with fluorescent mounting media containing DAPI (Abcam #104139) and glass coverslips. Immunofluorescence was visualized using a Leica SP8 (Leica) confocal microscope. Images were obtained with LASX (Leica) software. Secondary antibody specificity was confirmed by absence of signal in control samples stained without primary antibody. For quantification of SFTPC$^+$ pixel intensity and ACT$^+$ area fraction, confocal cross-section images of individual organoids were taken with identical contrast and brightness settings across treatment groups and imported into Image J. The outside perimeter of each organoid was used to define the region of interest for analyses. Antibodies used are listed in Table S2.

2.8. Re-sorting cells from organoid cultures

For re-sorting experiments, 200,000 mouse EpCAM$^+$ cells and 200,000 Mlg cells were seeded in 1 ml Matrigel diluted 1:1 with organoid culture medium into 6 well plates, and organoid culture medium was maintained on top. At the indicated time points, organoid cultures were digested with dispase for 30 min at 37 °C, and transferred to 15 ml tubes, washed with PBS, and digested further with trypsin for 5 min at 37 °C, prior to incubation with EpCAM microbeads (Miltenyi) and passed through LS columns. The EpCAM$^+$ and EpCAM$^-$ cell fractions were both used for RNA isolation and qRT-PCR analysis.

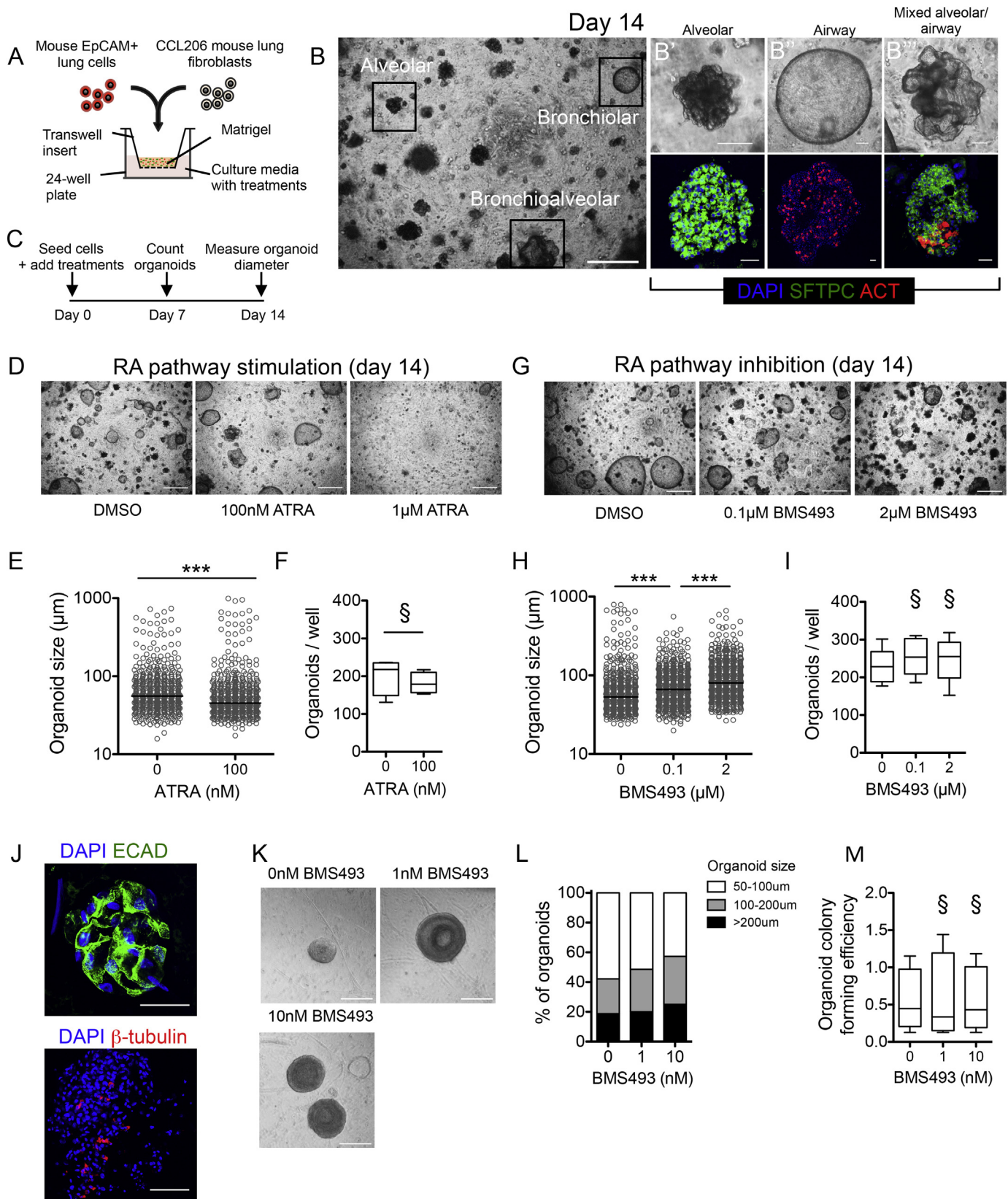## 2.9. Quantitative real-time polymerase chain reaction (qRT-PCR)

RNA was extracted from washed cell pellets using TriReagent (Life Technologies #AM9738) and trimethylene chlorobromide ([BCP], Sigma #B9673) followed by washing in isopropanol and elution in 30 μl RNAse-free ddH$_2$O. Total RNA concentrations were determined with a NanoDrop ND-1000 spectrophotometer. cDNA was synthesized using AMV reverse transcriptase (Promega, #A3500), and diluted with ddH$_2$O proportionately according to concentration of input RNA. qRT-PCR was performed with SYBR green (Roche, #04913914001) using Illumina Eco Real-Time PCR system. PCR cycling was follows: 94 °C for 30 s, annealing at 60 °C for 30 s, and extension at 72 °C for 30 s, for 40 cycles. qRT-PCR data were analyzed with LinRegPCR analysis software [42,43]. Geometric mean of the reference genes beta-2-microglobulin (B2M) and ribosomal protein L13A (RPL13A) was used to normalize qRT-PCR data. Primer sequences are listed in Table S3.

2.10. Statistical analysis

Data were analyzed with GraphPad Prism 5·0. Data are presented as mean ± SEM, or median (interquartile range) within the text. N refers to number of independent experiments starting from an independent EpCAM$^+$ isolation, and n refers to number of organoids. The statistical tests used are stated in the Figure legends. A value for p of <0·05 was considered significant.

3. Results

We investigated the regulation of adult lung epithelial progenitor growth and differentiation using an *in vitro* organoid (spheroid) assay, in which adult mouse distal lung EpCAM$^+$ epithelial cells were co-cultured with Mlg (CCL206) mouse lung fibroblasts in Matrigel (Fig. 1A) [5,40,41]. Organoids formed with an efficiency of $1 \cdot 1 \pm 0 \cdot 1\%$ per initial cells seeded, with distinct morphologies discernable by day 14 (Fig. S1A, 1B). Organoids exhibited morphology and immunofluorescence staining characteristic of alveolar (proSFTPC$^+$/ACT$^-$; Fig. 1B'), airway (proSFTPC$^-$/ACT$^+$; Fig. 1B") or mixed alveolar/airway (proSFTPC$^+$/

Day 14

DAPI SFTPC ACT

RA pathway stimulation (day 14)

DMSO   100nM ATRA   1μM ATRA

RA pathway inhibition (day 14)

DMSO   0.1μM BMS493   2μM BMS493

DAPI ECAD

DAPI β-tubulin

0nM BMS493   1nM BMS493

10nM BMS493

Organoid size
☐ 50-100um
▨ 100-200um
■ >200um

ACT^+; Fig. 1B‴) structures. By quantitative immunofluorescence $72 \cdot 0 \pm 5\%$ were alveolar, $8 \cdot 5 \pm 3\%$ were airway, $6 \cdot 8 \pm 3\%$ were mixed alveolar/airway, and $12 \cdot 7 \pm 4\%$ expressed neither marker (Fig. S1B).

Organoid cultures were incubated with pharmacological RA modulators and organoid number and diameter was measured at day 7 and 14, respectively (Fig. 1C). Organoids formed both in normal organoid media (containing 10 nM ATRA) and in ATRA-free media. ATRA-free media did not affect organoid size at day 14 compared to normal organoid media (Fig. S1C). When cultured in ATRA-free media, stimulation with ATRA (100 nM) from day 0 onwards significantly decreased

organoid size at day 14 (ATRA [0 nM] 55·8(42·4–84·6)μm; ATRA [100 nM] 44·6(36·1–66·5)μm, $p < 0.0001$; Fig. 1D,E). When categorized by morphology, the effect of ATRA was comparable in alveolar, airway and mixed alveolar/airway structures (Fig. S1D). Organoid number was not affected by ATRA (Fig. 1F). When cultured in normal organoid media, RA pathway inhibition with the pan-RAR inverse agonist BMS493 significantly increased organoid size (BMS493 [0 nM] 53·2 (41–76)μm; BMS493 [100 nM] 66·2(47·9–95·2)μm; BMS493 [2 μM] 80·2(57·4–118·3)μm; both $p < 0.0001$ vs [0 nM]; Fig. 1G,H). BMS493 increased size of alveolar, airway and mixed alveolar/airway structures (Fig. S1E). Organoid number was not affected by BMS493 (Fig. 1I).

To investigate the potential of RA pathway inhibition to promote human lung epithelial regeneration in COPD, EpCAM$^+$ cells were isolated from distal lung tissue obtained from 4 patients with moderate to severe COPD (GOLD Stage II-IV, patient characteristics are in Table S1) and cultured together with MRC5 human lung fibroblasts in Matrigel, which resulted in organoids forming with an efficiency of $0.54 \pm 0.2\%$. Immunofluorescence staining of human lung organoids at day 21 revealed positive staining for E-cadherin and β-tubulin indicating airway epithelial differentiation; proSFTPC could not be detected (Fig. 1J). Treatment with BMS493 reduced the frequency of smaller organoids (50-100 μm diameter) and increased the frequency of larger organoids (100-200 μm and > 200 μm; Fig. 1K, L). BMS493 did not affect organoid number (Fig. 1M). These data indicate that RA signaling is a conserved mechanism controlling growth of adult distal lung epithelial progenitor cells, and suggest that RA pathway inhibition can promote growth of epithelial progenitor cells in COPD lung.

3.1. RA pathway component gene expression during post-pneumonectomy lung regeneration

Our findings suggest that decreased RA pathway activity may correlate with epithelial proliferation during adult lung regeneration in vivo. We therefore interrogated a published microarray dataset of mouse lung samples taken either before (day 0) or at various time points following surgical pneumonectomy (day 3, 7, 14, 28, 56), to assess gene expression of RA receptors and proliferation markers during adult lung regeneration in vivo (GEO accession number GSE39817 [44],). Data from samples taken 56 days after sham surgery were included for comparison. Data are from cardiac and medial lobes, which exhibit the greatest growth and DNA synthesis following pneumonectomy [44]. As expected, proliferation markers (Mki67, Cdk1, Ccnb1, Mcm3, Mcm7) showed a clear upregulation at early time points compared to day 0, peaking at days 3 and 7, and normalizing to near baseline levels from day 14 onwards (Fig. S2A). Rara expression was relatively stable throughout the time course (Fig. S2B). Interestingly, Rarb expression showed the inverse trend to proliferation markers with a clear decrease from day 3 to 14, normalizing to near baseline levels from day 28 onwards (Fig. S2B). Rarg expression showed a modest decrease in the cardiac lobe at days 3 and 7 and a slight decrease in the medial lobe at day 3, normalizing thereafter (Fig. S2B). Gene expression trends in cardiac

and medial lobes were largely comparable for all genes. These data provide support to the notion that transient decrease in RA pathway activation is permissive for epithelial proliferation during adult lung regeneration in vivo.

3.2. RA signaling balances adult lung epithelial proliferation and differentiation

To investigate mechanisms of BMS493-induced lung organoid growth, treated mouse lung organoid cultures were enzymatically dissociated, and EpCAM$^+$ cells and fibroblasts were MACS-separated and subjected to gene expression analyses (Fig. 2A). RT-qPCR for the mesenchymal marker Vim and the epithelial marker Cdh1 on re-sorted cell fractions revealed enrichment for each cell type in their respective fraction (Fig. S3A). Re-sorting efficiency did not significantly differ between BMS493- or DMSO-treated cells (Fig. S3A). In both EpCAM$^+$ and fibroblast fractions re-isolated at day 7, BMS493 (2 μM) decreased mRNA expression of the RA pathway target gene Rarb (6·7 fold decrease in EpCAM$^+$ cells, 7·5 fold decrease in fibroblasts, both $p < 0.001$ vs control; Fig. 2B), which contains a RARE in its promoter region [45], confirming inhibition of RA signaling in both epithelial cells and fibroblasts by BMS493. As fibroblasts were proliferation-inactivated prior to culture, we investigated expression of cell cycle-related genes in EpCAM$^+$ cells; BMS493 increased expression of Cdk1, Ccnb1, Ccnd1 (Fig. 2C). RT-qPCR for cell survival regulators revealed that BMS493 decreased expression of the pro-apoptotic factor Bik in EpCAM$^+$ cells ($p < 0.05$ compared to DMSO; Fig. 2D), but did not alter Bcl2 or Bax expression (Fig. 2D). Immunofluorescence staining of day 7 organoid cultures revealed enrichment of Ki67$^+$ cells in both proSFTPC$^+$ and proSFTPC$^-$ organoids in BMS493-treated cultures compared to DMSO control (Fig. 2E), confirming induction of epithelial proliferation by BMS493.

We next investigated differentiation in lung organoid cultures. In EpCAM$^+$ cells re-isolated from control cultures at day 14, the most abundant transcript was Sftpc (Fig. S3B), in line with the predominance of alveolar organoids in culture (Fig. S1B). The next abundant were Scgb1a1 and FoxJ1 (Fig. S3B), suggesting the presence of airway organoids undergoing secretory and ciliated cell differentiation. Trp63 and Pdpn mRNA were detected at low levels, and Muc5ac mRNA was barely detected (Fig. S3B). BMS493 significantly decreased expression of Sftpc, Pdpn, Scgb1a1 and FoxJ1 (all $p < 0.05$ compared to DMSO control; Fig. 2F), whereas Trp63 showed a trend to decrease after BMS493, and Muc5ac was unchanged, which may reflect very low expression at baseline (Fig. 2F).

In organoids cultured in ATRA-free media, quantitative immunofluorescence revealed addition of ATRA caused an increase in the proportion of proSFTPC$^+$/ACT$^-$ alveolar organoids that did not reach statistical significance (ATRA [0 nM] $56.7 \pm 4\%$, ATRA [100 nM] $70.1 \pm 3\%$, $p = 0.0657$; Fig. 2G), with a concomitant significant decrease in proSFTPC$^-$/ACT$^-$ organoids (ATRA [0 nM] $25.5 \pm 3\%$, ATRA [100 nM] $12.1 \pm 1\%$, $p < 0.05$; Fig. 2G). ATRA-free media also decreased

Fig. 1. Retinoic acid signaling controls adult mouse and human distal lung epithelial organoid growth. A) Schematic of mouse organoid experimental setup, based on [5,40,41]. B) Representative low magnification light microscopy image of organoid culture at day 14, with distinct morphologies highlighted. Scale bar = 200 μm. Representative high magnification examples of B') alveolar, B") airway, and B"') mixed alveolar/airway morphologies by light microscopy (top) with corresponding immunofluorescence staining (bottom) for pro-surfactant protein C (SFTPC, green), acetylated tubulin (ACT, red), and DAPI (blue). Scale bars = 50 μm (top), 20 μm (bottom). C) Experimental plan. D-F) Effect of ATRA treatment on size and number of organoids cultured in ATRA-free media. D) Representative light microscopy images of organoid cultures treated with DMSO or with ATRA (0·1 μM, 1 μM). Scale bar = 200 μm. E) Quantification of organoid size at day 14 following treatment with DMSO or with ATRA (10 nM, 100 nM). $n > 510$ organoids per group from $N = 5$ independent isolations. Mann Whitney test, *** $p < 0.001$. F) Quantification of organoid number at day 7 treated with DMSO or with ATRA. Mann Whitney test, § p = not significant. G-I) Effect of RA pathway inhibition with the pan-RAR inverse agonist BMS493 on size and number of organoids cultured in media with 10 nM ATRA. G) Representative light microscopy images of organoid cultures treated with DMSO or with BMS493 (0·1 μM, 2 μM). Scale bar = 200 μm. H) Quantification of organoid size at day 14 following treatment without or with BMS493 (0·1 μM, 2 μM). $n > 570$ organoids per group from N = 5 independent isolations. Kruskall Wallis with Dunn's post test, *** p < 0.001. I) Quantification of organoid number at day 7 treated without or with BMS493. Kruskall Wallis with Dunn's post test, § p = not significant compared to BMS493 0 μM. J) Immunofluorescence images of human organoids at day 21 stained for E-cadherin (green) and β-tubulin (red), with DAPI (blue) as nuclear counterstain. Scale bars = 50 μm (top), 100 μm (bottom). K) Representative light microscopy images of human organoids at day 21 cultured with BMS493 (0, 1, 10 nM). Scale bars = 80 μm. L) Proportion of organoids 50-100 μm (white bars), 100-200 μm (grey bars), or > 200 μm (black bars) in diameter measured at day 21 after treatment with BMS493 (0, 10 nM, 10 nM). Bars represent sum of organoid counts pooled from 4 separate donors. M) Organoid colony forming efficiency of human organoids at day 14 after treatment with BMS493 (0, 1, 10 nM). Kruskall Wallis with Dunn's post test, § p = not significant compared to BMS493 0 nM. $N = 4$ donors. (For interpretation of the references to colour in this figure legend, the reader is referred to the web version of this article.)
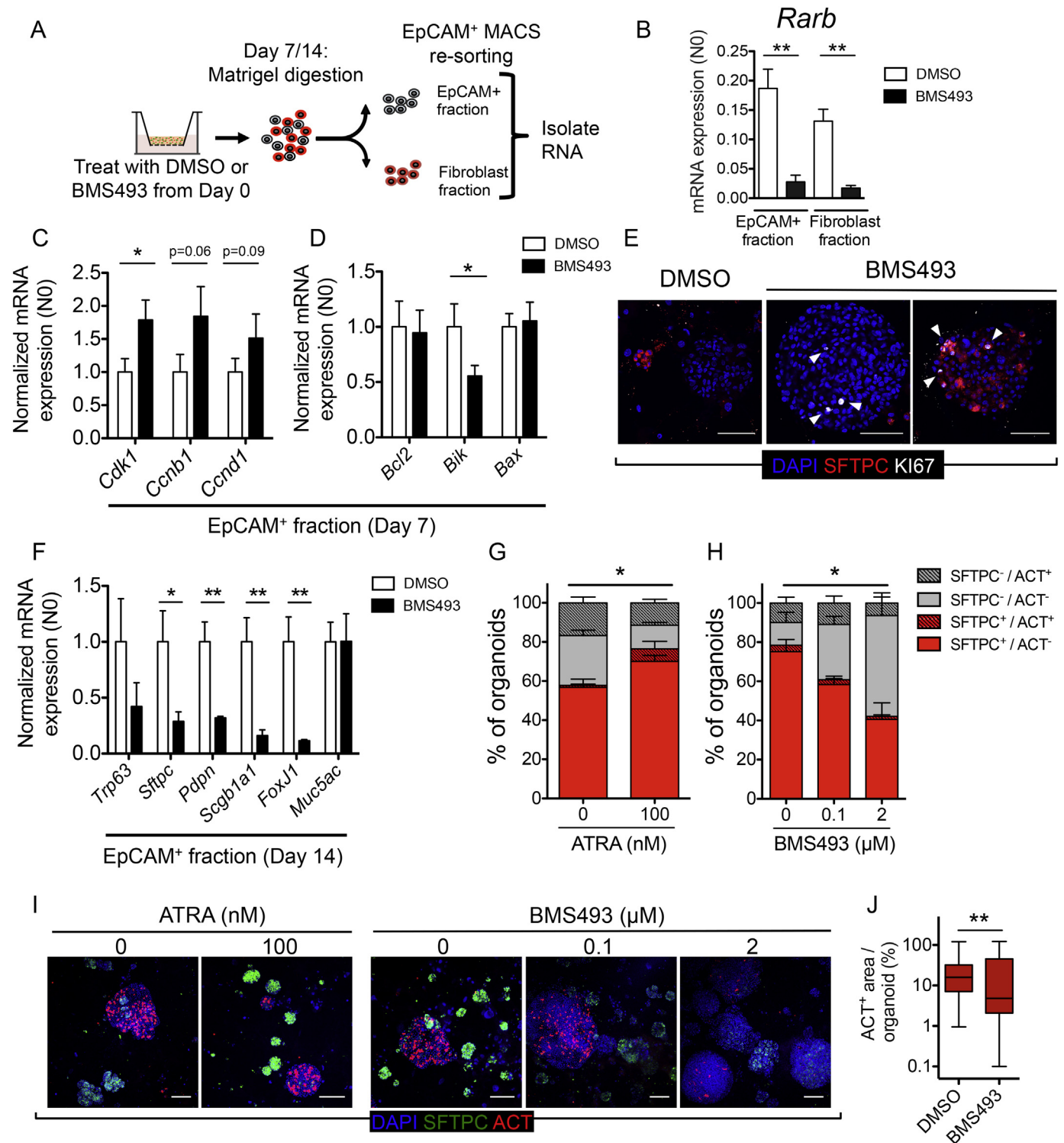
Fig. 2. Retinoic acid signaling balances lung progenitor cell proliferation and survival, and differentiation. A) Strategy to re-sort epithelial cells from fibroblasts in organoid cultures. B) RT-qPCR for *Rarb* in EpCAM[+] and fibroblast cells re-sorted at day 7, following either DMSO (white bars) or BMS493 (2 μM, black bars) treatment. N = 4 independent isolations. Unpaired *t*-test, ** $p < 0.001$ compared to corresponding DMSO control. C-D) RT-qPCR for C) cell cycle genes *Cdk1, Ccnb1* and *Ccnd1,* and D) cell survival genes *Bcl2, Bik* and *Bax,* in EpCAM^{+} cells re-sorted at day 7 following DMSO (white bars) or BMS493 (2 μM, black bars) treatment. N = 4 independent isolations. Paired t-test, * $p < 0.05$ compared to corresponding DMSO control. E) Representative immunofluorescence images of Ki67 staining (white) in organoids at day 7, showing enrichment (white arrows) in organoids following BMS493 treatment, in both alveolar (ProSFTPC[+], red), and non-alveolar organoids. DAPI (blue) was used as a nuclear counterstain (blue). Scale bar = 50 μm. F) RT-qPCR on EpCAM^{+} cells re-sorted from organoid cultures at day 14, showing effect of RA inhibition with BMS493 (2 μM, black bars) on mRNA expression of markers of specific lung cell types, compared to DMSO (white bars). N = 3–4 independent isolations. Unpaired t-test *$p < 0.05$, **$p < 0.01$ compared to corresponding DMSO control. G) Effect of ATRA (0, 100 nM, added to ATRA-free media) on proportion of organoids expressing SFTPC and/or ACT. N = 3 independent isolations. Unpaired t-test of total SFTPC[+] organoids, *$p < 0.01$. H) Effect of BMS493 (0, 0·1, 2 μM, added to normal culture media) on proportion of organoids expressing SFTPC and/or ACT. N = 3 independent isolations. One way ANOVA of SFTPC[+]/ACT[−] organoids with Dunnett's post test, *$p < 0.05$. I) Representative immunofluorescence images of day 14 organoid cultures treated with ATRA or BMS493, for SFTPC (green), ACT (red) and DAPI (blue). Scale bars = 100 μm. J) Digital quantification of ACT[+] area per organoid after BMS493 (2 μM) treatment. *n* > 46 organoids from 2 independent isolations. Mann Whitney test, **$p < 0.01$. (For interpretation of the references to colour in this figure legend, the reader is referred to the web version of this article.)

the proportion of alveolar organoids compared to normal organoid culture media (Fig. S4). Furthermore, when added to normal culture media, BMS493 decreased the proportion of alveolar organoids (BMS493 [0 μM] 75·2 ± 6%, BMS493 [0·1 μM] 58·4 ± 4%, BMS493 [2 μM] 40·1 ± 9%, [2 μM] p < 0·05 compared to [0 μM]; Fig. 2H), and increased the proportion of proSFTPC⁻/ACT⁻ organoids (BMS493 [0 μM] 11·5 ± 5%, BMS493 [0·1 μM] 28·2 ± 4%, BMS493 [2 μM] 51·5 ± 12%, [2 μM] p < 0·05 compared to [0 μM]; Fig. 2H). Additionally, proSFTPC staining intensity was increased by ATRA, and decreased by BMS493 (Fig. 2I). The proportion of proSFTPC⁻/ACT⁺ or proSFTPC⁺/ACT⁺ organoids was unchanged by either ATRA or BMS493 (Fig. 2H). However, BMS493 treatment significantly reduced the ACT⁺ area per organoid, indicating reduced numbers of airway ciliated cells (BMS493 [0 μM] 15·9 [7–32]%, BMS493 [2 μM] 4·8 [2–46]%, p < 0·01; Fig. 2I, J). Altogether, these data suggest RA pathway inhibition promoted adult distal lung epithelial progenitor cell proliferation while suppressing proper alveolar and airway differentiation, whereas RA pathway stimulation had the inverse effects.

3.3. RA pathway inhibition promotes lung organoid proliferation via YAP pathway activation

To investigate downstream molecular pathways that mediate increased lung epithelial growth after RA pathway inhibition, we focused on Yes-associated protein (YAP), a transcriptional co-activator that controls organ size during development by regulating gene expression together with the TEAD family of nuclear transcription factors [46,47]. RT-qPCR for a selection of YAP target genes [48] revealed activation of YAP signaling in EpCAM⁺ cells by BMS493 (*Tead4*, *Kif23*, *Polh*, *Ccna2* p < 0·05, and *Cdca5*, *Cdca8* p < 0·01 compared to DMSO control; Fig. 3A). Gene expression of *Yap* and the closely related transcriptional co-activator *Taz* were unchanged by BMS493 (Fig. 3B). We used immunofluorescence for YAP protein to investigate subcellular localization, which revealed nuclear YAP localization and thus YAP pathway activation in both proSFTPC⁺ and proSFTPC⁻ organoids following BMS493, where it frequently co-localized with Ki67 (Fig. 3C). Quantitative immunofluorescence showed that ATRA decreased the proportion of organoids at day 7 with nuclear YAP (ATRA [0 nM] 41·3 ± 17%, ATRA
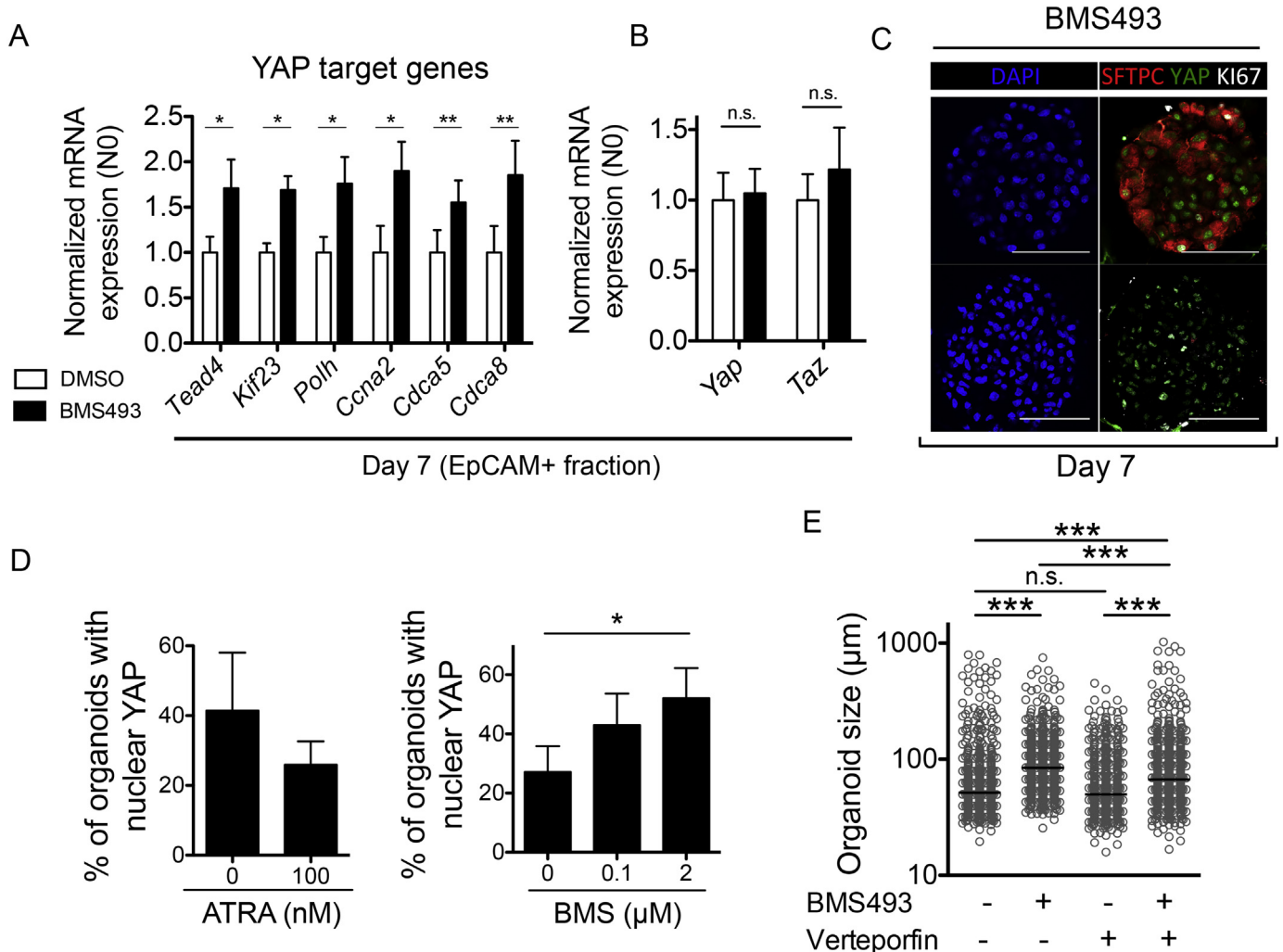

Fig. 3. Retinoic acid signaling controls lung organoid size *via* epithelial yes-associated protein (YAP) pathway. A-B) RT-qPCR on EpCAM⁺ cells re-sorted from organoid cultures at day 7, for A) YAP pathway target genes, or B) *Yap* and *Taz*, following treatment with DMSO vehicle (white bars) or BMS493 (2 μM; black bars). N = 4 independent isolations. Paired t-test, *p < 0·05, **p < 0·01 compared to corresponding DMSO control. C) Representative immunofluorescence images of day 14 organoid cultures treated with BMS493 (2 μM), for SFTPC (red), Yap (green), and Ki67 (white), showing an alveolar (top) and non-alveolar (bottom) organoid. DAPI was used as a nuclear counterstain (blue). Scale bars = 50 μm. D) Quantification of proportion of organoids exhibiting nuclear Yap protein following ATRA (0, 100 nM, added to ATRA-free media, left), or BMS493 (0, 0·1, 2 μM added to normal culture media, right). Kruskal Wallis with Dunn's post test, *p < 0·05. E) Organoid diameter, measured at day 14, following treatment with DMSO, or BMS493 (2 μM) or the Yap pathway inhibitor verteporfin (4 μM) alone in combination. *n* > 545 organoids per group, N = 5 independent isolations. Kruskall Wallis with Dunn's post test, *** p < 0·001. (For interpretation of the references to colour in this figure legend, the reader is referred to the web version of this article.)
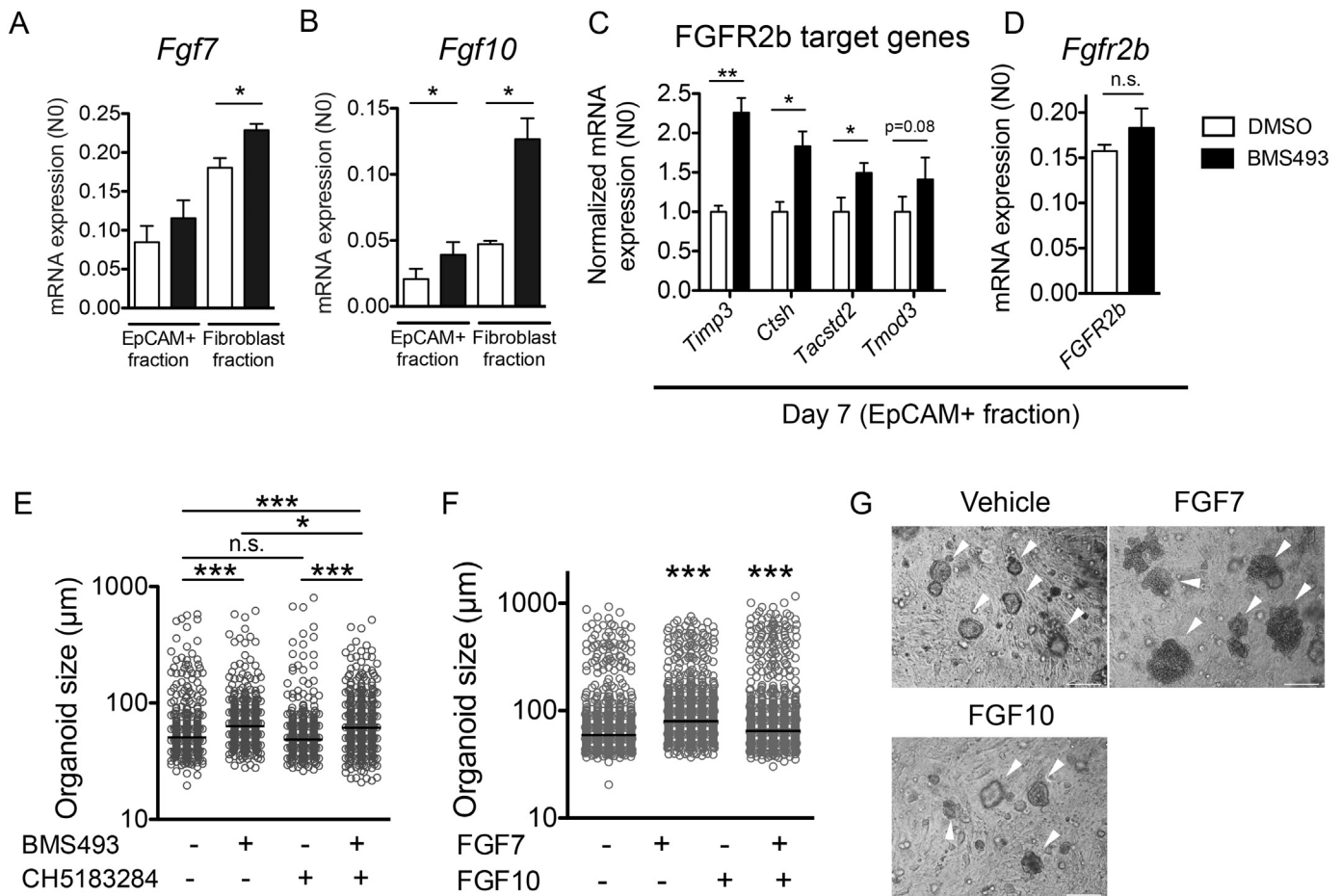
Fig. 4. Fibroblast-epithelial FGF-FGFR2b signaling contributes to growth induced by RA inhibition. A) RT-qPCR for A) *Fgf7* and B) *Fgf10* in EpCAM$^+$ and fibroblast cells re-sorted at day 7, following either DMSO (white bars) or BMS493 (2 μM, black bars) treatment. N = 4 independent isolations. Paired t-test, *p < 0·05, ** p < 0·001 compared to corresponding DMSO control. C-D) RT-qPCR on EpCAM$^+$ cells re-sorted from organoid cultures at day 7, for C) FGFR2b target genes, or D) *Fgfr2b*, following treatment with DMSO vehicle (white bars) or BMS493 (2 μM; black bars). N = 4 independent isolations. Paired t-test, n.s. = not significant. *p < 0·05, **p < 0·01 compared to corresponding DMSO control. E) Organoid diameter, measured at day 14, following treatment with DMSO control, or BMS493 (100 nM) or the pan-FGFR inhibitor CH5183284 (100 nM) alone or in combination. n > 374 organoids per group, N = 3 independent isolations. Kruskall Wallis with Dunn's post test, *p < 0·05, *** p < 0·001. F) Organoid diameter, measured at day 14, following treatment with vehicle, recombinant FGF7 (50 ng/ml) or recombinant FGF10 (100 ng/ml). n > 900 organoids per group, N = 3 independent isolations. Kruskall Wallis with Dunn's post test, *** p < 0·001. G) Representative light microscopic images of day 14 organoid cultures showing effect of recombinant FGF7 and FGF10 on organoid size (arrowheads). Scale bars = 80 μm.

[100 nM] 25·9 ± 7%; Fig. 3D), whereas BMS493 increased proportion of organoids with nuclear YAP (BMS493 [0 μM] 27·2 ± 9%, BMS493 [0·1 μM] 43·0 ± 11, BMS493 [2 μM] 52·1 ± 10%, BMS [2 μM] p < 0·05 compared to BMS [0 μM]; Fig. 3D). Together, these data indicate that RA inhibition with BMS493 leads to epithelial YAP pathway activation.

We next investigated the role of YAP pathway in BMS493-induced epithelial proliferation by treating organoid cultures with BMS493 (2 μM) or the YAP pathway inhibitor verteporfin (4 μM) [49] alone or combined. Verteporfin alone had no effect on organoid size or number compared to DMSO control (Fig. 3E and data not shown), whereas verteporfin prevented BMS493-induced increase in organoid size (BMS493 84·4(60–121)μm, BMS493 + verteporfin 67·0(49–110)μm, p < 0·001; Fig. 3E). These data suggest that RA inhibition promotes mouse lung organoid growth *via* YAP nuclear translocation and transcription of YAP target genes.

3.4. Fibroblast-epithelial FGF signaling contributes to lung organoid growth after RA inhibition

The presence of both epithelial cells and fibroblasts in organoid cultures raised the possibility that RA inhibition caused epithelial growth *via* indirect effects on fibroblasts. FGF7 and FGF10 are mesenchyme-derived signaling molecules important for epithelial growth during lung development and adult lung repair [40,50–53], and in mouse

lung development, RALDH2 downregulation, causing reduced RA signaling, induced FGF10 in the distal tip mesenchyme to allow proper epithelial branching [16]. We therefore focused on fibroblast-epithelial FGF signaling as a potential mechanism of BMS493-induced lung organoid growth. BMS493 significantly increased gene expression of both *Fgf7* and *Fgf10* in fibroblasts re-isolated from organoid cultures at day 7 (p < 0·05 compared to DMSO control; Fig. 4A, B). BMS493 also caused a modest significant induction of *Fgf10* in the EpCAM$^+$ fraction (p < 0·05; Fig. 4B). BMS493 induced expression of FGFR2b pathway target genes [54] within the EpCAM$^+$ fraction (*Timp3* p < 0·01, *Ctsh* p < 0·05, *Tacstd2* p < 0·05, *Tmod3* p = 0·08, BMS493 compared to DMSO control; Fig. 4C). Gene expression of *Fgfr2b* was unchanged by BMS493 (Fig. 4D). These data suggest that FGF7/10-FGFR2b fibroblast-epithelial signaling may contribute to growth induction by RA pathway inhibition. To investigate this, organoid cultures were treated with BMS493 (100 nM) or the FGFR inhibitor CH5183284 (100 nM), alone or in combination, for 14 days. CH5183284 alone did not affect organoid size compared to DMSO control (Fig. 4E), whereas CH5183284 partially prevented BMS493-induced increase in organoid size (BMS493 63·2 (51–84)μm, CH5183284 + BMS493 61·4(45–83)μm, p < 0·05; Fig. 4E). Next, the effect of recombinant human FGF7 and FGF10 on organoid size was investigated. Recombinant FGF7 led to a significant increase in organoid size compared to vehicle control (vehicle 59·3 (50–76)μm, FGF7 80·0(62–112)μm, p < 0·001; Fig. 4F, G). FGF10 also

significantly increased organoid size, although to a lesser extent than FGF7 (FGF10 64·8(52–90)μm, p < 0·001; Fig. 4F, G). These data provide further support for the notion that enhanced epithelial growth in mouse lung organoids following RA pathway inhibition may be mediated in part by fibroblast-epithelial FGF signaling.

3.5. HDAC inhibition as a strategy to rescue lung epithelial differentiation after RA inhibition

We next investigated strategies to rescue organoid differentiation following pharmacological RA pathway inhibition. BMS493 inhibits RA signaling by stabilizing the association between DNA-bound RAR/RXR heterodimers and nuclear receptor co-repressor (NCoR) [55], part of a co-repression complex that contains histone deacetylases (HDACs). HDACs mediate transcriptional repression by maintaining chromatin in a condensed state. We reasoned that after BMS493 treatment, subsequent addition of a pharmacological HDAC inhibitor would inhibit the activity of the stabilized co-repression complex, permitting chromatin remodeling and de-repression of RA target genes and thus enable proper differentiation. To investigate this, organoid cultures were treated with BMS493 for 14 days, or for 7 days followed by a washout period with culture media containing either 10 nM ATRA or 100 nM ATRA, supplemented either with DMSO or with the pan-HDAC inhibitor SAHA (Fig. 5A). Organoid cultures treated with DMSO for 14 days served as controls. All treatment groups led to significantly increased organoid size compared to DMSO control (all p < 0·001 compared to DMSO; Fig. 5B). Notably, the size of organoids in cultures treated with BMS493 for 14 days was not significantly different to those treated for 7 days (Fig. 5B). Additionally, SAHA treatment from day 7 did not have a significant effect on organoid size compared to the corresponding DMSO control (Fig. 5B). Morphologically, BMS493 treatment for 14 days gave rise to organoids with a dark, dense appearance with irregular edges suggestive of an immature state (Fig. 5C). Reducing BMS493 treatment to 7 days followed by a 7 day washout with 100 nM ATRA did not restore organoid morphology. However, treatment with SAHA +100 nM ATRA from day 7 restored organoids to regular morphologies observed in control cultures (Fig. 5C).

BMS493 treatment for 14 days strongly reduced *Rarb* expression in the EpCAM+ fraction (p < 0·001 compared to DMSO control; Fig. 5D). Notably, 7 days of BMS493 treatment followed by 7 day washout with either 10 nM or 100 nM ATRA did not restore *Rarb* expression, indicating lasting repression of RA signaling by BMS493, likely *via* epigenetic silencing. Addition of SAHA to medium with 10 nM ATRA had no effect on *Rarb* expression. However, addition of SAHA to medium containing 100 nM ATRA significantly increased *Rarb* expression (p < 0·01 compared to BMS493 [14 days]; Fig. 5D), indicating partial restoration of RA signaling. We therefore investigated the impact of BMS493 washout with SAHA +100 nM ATRA on organoid differentiation.

RT-qPCR revealed repression of *Sftpc*, *Scgb1a1*, *FoxJ1* and *Pdpn* gene expression by 14 days BMS493 treatment, which was not restored by washout with 100 nM ATRA alone (Fig. 5E). Interestingly, washout with SAHA +100 nM ATRA from day 7 led to a significant increase in *Scgb1a1* mRNA expression (p < 0·05 compared to BMS493 [14 days]; Fig. 5E). *Sftpc*, *FoxJ1* and *Pdpn* expression were not changed by SAHA (Fig. 5E). *Muc5ac* gene expression was unchanged by 14 days of BMS493 or 7 days of BMS493 followed by 7 day washout with 100 nM ATRA, but was significantly decreased by SAHA +100 nM ATRA (p < 0·05 compared to BMS493 [14 days]; Fig. 5E).

Immunofluorescence and digital quantification of proSFTPC+ staining intensity revealed that BMS493 followed by washout reduced proSFTPC protein expression (Fig. 5F; DMSO 117·3(82–223), BMS493 64·7 [42–84], p < 0·001; Fig. 5G). Addition of SAHA in the washout period significantly increased proSFTPC protein (SAHA 93·0(67–135), p < 0·01 SAHA compared to BMS493 alone; Fig. 5G), suggesting that SAHA rescued AT2 differentiation following RA pathway suppression. SAHA did not affect the proportion of proSFTPC+ organoids (Fig. 5H).
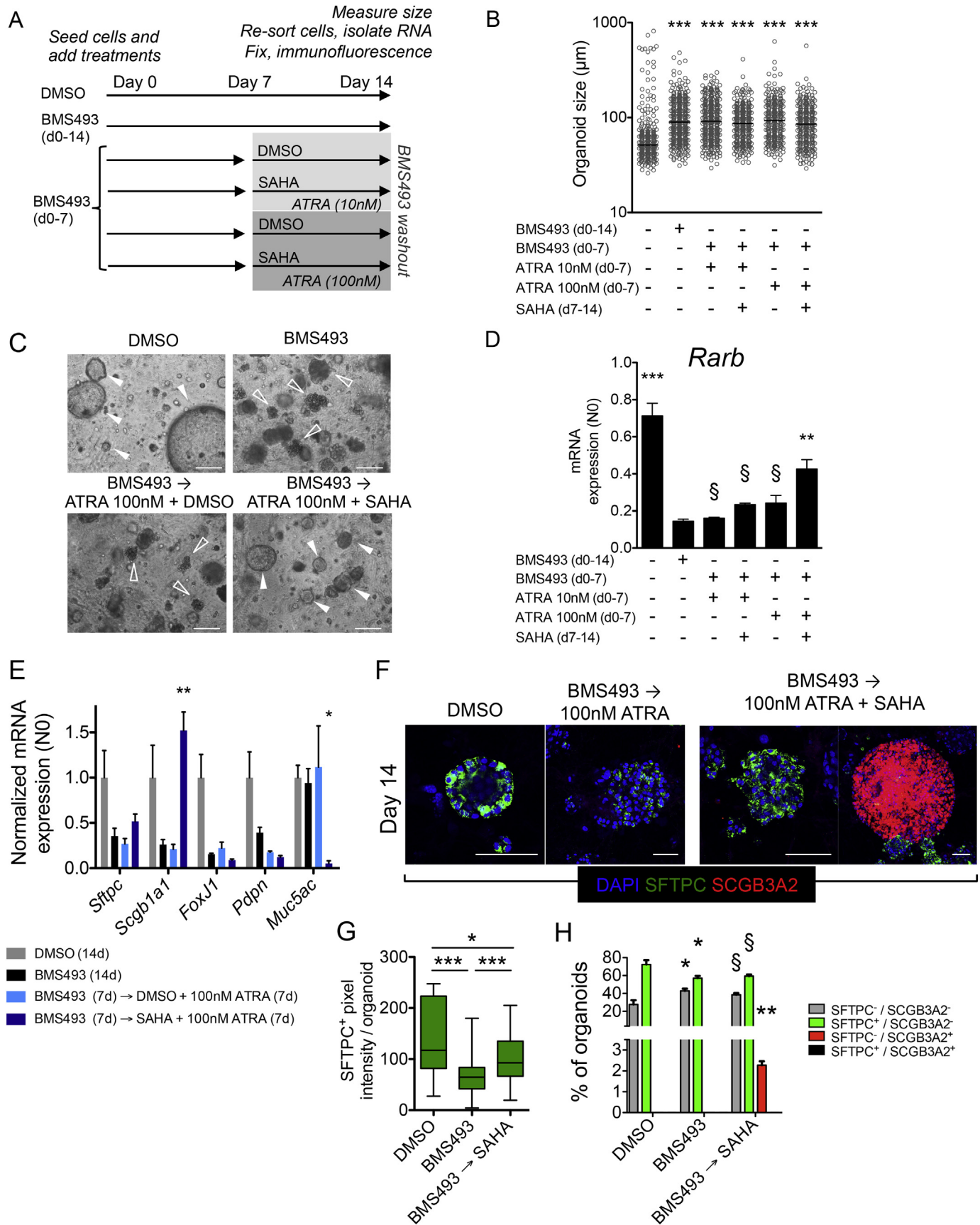
Unexpectedly, SAHA treatment induced protein expression of the club cell marker SCGB3A2 in proSFTPC− organoids, which was not observed either in cultures treated with DMSO or BMS493 alone (SAHA 2·3 ± 0·2%, p < 0·001 compared to DMSO and BMS493; Fig. 5F, H). Altogether, these data suggest that HDAC inhibition combined with ATRA restored RA signaling following BMS493 treatment, and rescued differentiation of AT2 and club cells.

4. Discussion

RA signaling has received interest as a potential therapeutic target for chronic lung diseases, in part due to pre-clinical studies using *in vivo* models of COPD/emphysema that found induction of alveolar regeneration by ATRA administration [25–32]. The failure of retinoids in clinical trials for emphysema patients has been difficult to explain [33–36], in part because the specific role of RA signaling in adult distal lung epithelial progenitor cells has been little explored. Using an adult lung epithelial organoid model, we unexpectedly found that ATRA decreased lung organoid size, whereas RA pathway inhibition increased size of mouse lung organoids and of organoids derived from COPD patient lung tissue. In mouse lung organoids, RA inhibition augmented lung epithelial proliferation while suppressing airway and alveolar differentiation, and was mediated by epithelial YAP pathway activation and fibroblast-epithelial FGF signaling. HDAC inhibition combined with ATRA restored RA signaling and rescued alveolar and airway differentiation. Thus, rather than RA pathway stimulation, our study suggests therapeutic potential for controlled, transient RA pathway inhibition followed by pharmacological induction of differentiation to promote lung epithelial regeneration in chronic lung diseases.

Our findings are surprising, as induction of alveolar regeneration by ATRA *in vivo* presumably requires lung epithelial proliferation [25–32]. A possible explanation is that adult lung cell types present *in vivo* but not represented in the organoid assay could modulate the epithelial response to ATRA. An inherent limitation of the organoid assay is loss of cell-cell contacts between epithelial cells and other lung cell types including endothelial and immune cells; for example, lung endothelial cells instructed alveolar differentiation of epithelial cells in organoid co-cultures [56]. An alternative explanation is that ATRA administration *in vivo* could cause a transient increase in RA pathway inhibition *via* induction of CYP26 enzymes that catalyze the breakdown of RA; CY26A1 is highly inducible by RA due to presence of multiple RAREs in its promoter region [57]. In mouse embryos, ATRA administration paradoxically phenocopied the teratogenic effects of targeted RALDH2 or compound RAR disruptions, through induction of CYP26A1 and CYP26B1 and consequent RA pathway inhibition [58–60]. Consistent with the idea that RA pathway inhibition is permissive for epithelial proliferation *in vivo*, our analysis of a published microarray dataset [44] revealed that decreased *Rarb* expression coincided with the proliferative phase of post-pneumonectomy lung regeneration.

The transcriptional program induced by RA is highly developmental stage and cell type specific, and may promote or inhibit growth of adult cells depending on cell type [14]. Our findings suggest RA signaling represses growth of normal adult distal lung epithelial progenitor cells, as has previously been shown in small cell lung cancer cells [61] and immortalized human bronchial epithelial cells [62]. BMS493 increased size but did not affect number of epithelial organoids derived from resected lung tissue from COPD patients, suggesting conservation of this mechanism in adult human lung epithelium. Notably, BMS493 strongly repressed *Rarb* expression. While *Rarb* expression is widely used to report RA pathway activity due to an RARE in its promoter region [45], RARβ is also recognized as a tumor suppressor [63–65] and its expression is frequently perturbed in human lung cancer [66,67]. The specific transcriptional repertoire controlled by RARβ has yet to be fully characterized in lung epithelial progenitor cells. RA inhibition in lung organoids reduced expression of *Bik*, which encodes a pro-apoptotic member of the Bcl2 family of cell survival proteins [68], suggesting RA

A. Seed cells and add treatments / Measure size, Re-sort cells, isolate RNA, Fix, immunofluorescence

B. Organoid size (µm)

C. DMSO, BMS493, BMS493 → ATRA 100nM + DMSO, BMS493 → ATRA 100nM + SAHA

D. *Rarb* mRNA expression (N0)

E. Normalized mRNA expression (N0): Sftpc, Scgb1a1, FoxJ1, Pdpn, Muc5ac

DMSO (14d); BMS493 (14d); BMS493 (7d) → DMSO + 100nM ATRA (7d); BMS493 (7d) → SAHA + 100nM ATRA (7d)

F. Day 14 — DMSO, BMS493 → 100nM ATRA, BMS493 → 100nM ATRA + SAHA. DAPI SFTPC SCGB3A2

G. SFTPC+ pixel intensity / organoid: DMSO, BMS493, BMS493 → SAHA

H. % of organoids: SFTPC⁻/SCGB3A2⁻, SFTPC⁺/SCGB3A2⁻, SFTPC⁻/SCGB3A2⁺, SFTPC⁺/SCGB3A2⁺

signaling may regulate apoptosis in adult lung epithelial cells. Consistent with this, ATRA induced Bik expression in acute promyelocytic leukemia cells [69] and regulated expression of other Bcl2 family members in various cancer cell types [63].

Our findings suggest YAP pathway activation contributed to augmented epithelial proliferation in mouse lung organoids following RA pathway inhibition. The YAP pathway appears to be a common nodal point integrating pro-growth stimuli, as YAP activation regulated AT2 cell proliferation during lung regeneration following pneumonectomy in adult mice [70], and promoted adult mouse airway epithelial cell proliferation *in vivo* and *in vitro* [71–73]. Notably, YAP hyperactivity is widely associated with human malignancies including lung cancer [74], and YAP activation contributed to lung cancer progression in adult mice *in vivo* [75,76]. The mechanism by which RA signaling restricts YAP activity to control lung epithelial proliferation is currently unclear. We found that FGFR inhibition partially prevented mouse lung organoid growth induced by BMS493, and recombinant FGF7 and FGF10 mirrored the effect of BMS493, suggesting that RA inhibition may drive YAP pathway activity *via* fibroblast-derived FGF7 and FGF10 signaling to epithelial FGFR2b. Additionally, BMS493 induced *Fgf7* and *Fgf10* gene expression in fibroblasts, suggesting RA signaling normally represses their expression in lung mesenchyme. Consistent with this, *Raldh2* downregulation was required for mesenchymal *Fgf10* induction in the distal tip of branching airways during mouse lung development [16]. FGFR2-mediated signaling was previously described to interact with YAP and control its activity [77], however, other transcription factors and signaling molecules may also function downstream of RA signaling to control YAP activity [78]. Further studies using human models are needed to investigate the relevance of YAP and FGFR-mediated pathways downstream of RA signaling in human lung epithelium.

RA pathway modulation affected the proportion of alveolar organoids and the number of ACT$^+$ ciliated cells per organoid, implicating RA signaling in the control of adult alveolar and airway epithelial differentiation. This is in line with described effects of RA pathway activation in inducing differentiation of both embryonic and adult stem/progenitor cell types [79–83]. RA is well known to promote mucociliary differentiation of adult airway epithelial cells *in vitro* [84,85], and RA deficiency in adult rats caused airway epithelial squamous metaplasia that was reversed by vitamin A supplementation [86]. Further investigations into RAR subtypes that control alveolar and airway differentiation in adult lung epithelial cells may aid in development of specific, targeted retinoid lung regenerative therapies.

Typically, ATRA binding to RAR/RXR heterodimers displaces co-repressors for a co-activator complex containing histone acetyltransferases (HATs) to allow chromatin remodeling at receptor-targeted loci and enable transcription [14]. BMS493 washout followed by addition of 100 nM ATRA did not restore expression of *RARb* or of lung epithelial cell markers, suggesting that BMS493 caused lasting chromatin compaction at genes required for differentiation [55]. Accordingly, HDAC inhibition combined with ATRA partially restored *RARb* expression in BMS493-treated organoids, and increased protein expression of proSFTPC and SCGB3A2, suggesting restoration of alveolar and airway differentiation. Notably, HDACs enhanced the differentiation-inducing ability of RA in

neuroblastoma *in vitro* and *in vivo* [87] and the combination of HDACs and retinoids has been explored in clinical trials for solid tumors and hematologic malignancies [88,89]. Whether ATRA-induced differentiation in adult lung epithelial progenitor cells arises through direct transcription of RAR target genes or indirectly *via* secondary transcription factors remains to be determined [90]; investigations into genome-wide chromatin occupancy of ATRA-RAR complexes in specific lung epithelial cell types might be informative. Furthermore, the specific role of HDACs in lung epithelial differentiation, and whether this is either influenced by prior RA pathway inhibition, or depends on concomitant RA pathway activation, warrants further study. *Muc5ac* expression was further repressed by HDAC inhibition, suggesting goblet cell differentiation may require HDAC activity. Additionally, inhibited differentiation after BMS493 treatment may involve epithelial YAP pathway activation, as YAP phosphorylation and cytoplasmic sequestration was critical for airway epithelial secretory and ciliated cell differentiation [71,72].

A potential limitation to our study is that BMS493 promotes chromatin compaction at RAR-targeted loci, and thus may repress RA target genes that would normally be activated independent of RA signaling; consequently, BMS493 could elicit different effects than absence of ATRA alone. In support of an RAR-specific mechanism of BMS493, reduced alveolar differentiation following BMS493 mirrored the effect ATRA-free media. However, unlike BMS493 treatment, ATRA-free media did not significantly affect organoid size compared to normal culture media, which contains 10 nM ATRA. Retinoids have been identified in fetal bovine serum [91], which could have been sufficient to repress growth in absence of exogenous ATRA. Additionally, human bronchial epithelial cells can esterify retinol for intracellular storage, which could mitigate the effect of ATRA exclusion in our study [92]. Nonetheless, 100 nM ATRA reduced organoid size, supporting the notion that epithelial growth is controlled by RA signaling.

RA inhibition promoted growth of organoids derived from human lung cells isolated from lung tissue from end-stage COPD patients, supporting the idea that RA pathway inhibition may hold therapeutic potential to induce epithelial regeneration in human severe chronic lung disease. Further optimization of human lung organoid culture to allow alveolar differentiation will be necessary to understand the relevance of these findings to human alveolar repair. Additionally, our data suggest potential for RA pathway inhibition for *in vitro* expansion of lung epithelial progenitor cells for regenerative cell-based strategies. Prospective selective therapies using RA pathway inhibition must be carefully controlled to allow appropriate re-activation of RA signaling for correct differentiation. In light of the high frequency of both RA pathway and YAP pathway perturbations in lung cancer [66,67,74], the mechanism by which RA inhibition permits YAP activation and promotes lung epithelial proliferation warrants further investigation. *In vitro*, ATRA stimulated lung microvascular angiogenesis [20] and lung fibroblast elastin synthesis [21], and thus non-epithelial cellular processes critical for lung regeneration may require RA pathway activation. Further studies are needed to investigate the balance of RA pathway activation and inhibition required for lung regeneration, the timing of pathway modulation, and the specific role of RA signaling in other relevant lung cell types. As RA pathway perturbations have been identified in emphysematous lung tissue and cells isolated from COPD

Fig. 5. HDAC inhibition promotes differentiation following RA inhibition-induced growth. A) Experimental plan. B) Organoid diameter, measured at day 14, following treatment with DMSO or the indicated treatments. $n > 289$ organoids per group, $N = 2$ independent isolations. Kruskall Wallis with Dunn's post test, *** $p < 0·001$ compared to DMSO control, all other between-group comparisons were not significant. C) Representative light microscopic images of day 14 organoid cultures showing effect of the indicated treatments. BMS493 treatment caused an immature organoid morphology that was not restored by a washout period with 100 nM ATRA (empty arrowheads). Addition of SAHA in the washout period restored organoid morphology to similar to DMSO control (white arrowheads). Scale bars = 80 μm. D) RT-qPCR for *Rarb* on EpCAM$^+$ cells re-sorted from organoid cultures at day 14 after treatment with DMSO or the indicated treatments. N = 2–3 independent isolations. One way ANOVA with Bonferroni's post-test, ***$p < 0·001$, **$p < 0·01$ compared to BMS493 (d0-d14). E) RT-qPCR for lung epithelial cell type markers in EpCAM$^+$ cells re-sorted from organoid cultures at day 14 after treatment with DMSO or the indicated treatments. N = 3–6 independent isolations. One way ANOVA with Dunnett's post-test, **$p < 0·01$, *$p < 0·05$ compared to corresponding DMSO (14d) control. F) Representative immunofluorescence images of day 14 organoids showing effect of the indicated treatments on SFTPC (green) and SCGB3A2 (red) protein expression, with DAPI (blue) as nuclear counterstain. Scale bars = 50 μm. G) Digital quantification of SFTPC+ staining pixel intensity per organoid from day 14 organoid cultures after the indicated treatments. $n > 47$ organoids, N = 3 independent isolations. Kruskall Wallis with Dunn's post test, *** $p < 0·001$, *$p < 0·05$ compared to DMSO control. H) Effect of the indicated treatments on proportion of organoids expressing SFTPC and/or SCGB3A2. N = 3 independent isolations. One way ANOVA with Dunnett's post test, ** $p < 0·01$, *$p < 0·05$, § = not significant compared to corresponding DMSO control. (For interpretation of the references to colour in this figure legend, the reader is referred to the web version of this article.)

patients [20,24], additional studies investigating the potential of RA pathway modulation to augment repair in human models using epithelial cells and fibroblasts from COPD patients are required, particularly as animal models of COPD may not fully recapitulate human disease [93]. Furthermore, the regenerative competence of the COPD lung, including the extent to which relevant progenitor cell types and regenerative signaling pathways remain intact in diseased lung tissue, requires better characterization for successful application of retinoid-based regenerative therapies.

Funding

Declaration of interests

All authors have no competing interests to declare, financial or otherwise.

Author contributions

JPNB: Conception and design, collection and assembly of data, data analysis and interpretation, manuscript writing, critical reading and revision, final approval of manuscript.

AS: Collection and assembly of data, data analysis and interpretation, critical reading and revision, final approval of manuscript.

RK: Collection and assembly of data, data analysis and interpretation, critical reading and revision, final approval of manuscript.

IHH: Collection and assembly of data, critical reading and revision, final approval of manuscript.

JAN: Collection and assembly of data, critical reading and revision, final approval of manuscript.

PSH: Conception and design, data analysis and interpretation, financial support, manuscript writing, critical reading and revision, final approval of manuscript.

JS: Conception and design, data analysis and interpretation, financial support, manuscript writing, critical reading and revision, final approval of manuscript.

MK: Conception and design, data analysis and interpretation, financial support, manuscript writing, critical reading and revision, final approval of manuscript.

RG: Conception and design, data analysis and interpretation, financial support, manuscript writing, critical reading and revision, final approval of manuscript.

Appendix A. Supplementary data

Supplementary data to this article can be found online at https://doi.org/10.1016/j.ebiom.2018.09.002.

References

[1] Rabe KF, Watz H. Chronic obstructive pulmonary disease. Lancet 2017 May 13;389 (10082):1931–40 [PubMed PMID: 28513453].

[2] Vogelmeier CF, Criner GJ, Martinez FJ, Anzueto A, Barnes PJ, Bourbeau J, et al. Global Strategy for the diagnosis, management, and prevention of chronic obstructive lung disease 2017 report. GOLD executive summary. Am J Respir Crit Care Med 2017 Mar 1;195(5):557–82 [PubMed PMID: 28128970].

[3] Hogan BL, Barkauskas CE, Chapman HA, Epstein JA, Jain R, Hsia CC, et al. Repair and regeneration of the respiratory system: complexity, plasticity, and mechanisms of lung stem cell function. Cell Stem Cell 2014 Aug 07;15(2):123–38 [PubMed PMID: 25105578. Pubmed Central PMCID: 4212493].

[4] Rawlins EL, Okubo T, Xue Y, Brass DM, Auten RL, Hasegawa H, et al. The role of Scgb1a1+ Clara cells in the long-term maintenance and repair of lung airway, but not alveolar, epithelium. Cell Stem Cell 2009 Jun 5;4(6):525–34 [PubMed PMID: 19497281. Pubmed Central PMCID: 2730729].

[5] Barkauskas CE, Cronce MJ, Rackley CR, Bowie EJ, Keene DR, Stripp BR, et al. Type 2 alveolar cells are stem cells in adult lung. J Clin Invest 2013 Jul;123(7):3025–36 [PubMed PMID: 23921127. Pubmed Central PMCID: 3696553].

[6] Zuo W, Zhang T, Wu DZ, Guan SP, Liew AA, Yamamoto Y, et al. p63(+)Krt5(+) distal airway stem cells are essential for lung regeneration. Nature 2015 Jan 29;517(7536): 616–20 [PubMed PMID: 25383540].

[7] Vaughan AE, Brumwell AN, Xi Y, Gotts JE, Brownfield DG, Treutlein B, et al. Lineage-negative progenitors mobilize to regenerate lung epithelium after major injury. Nature 2015 Jan 29;517(7536):621–5 [PubMed PMID: 25533958. Pubmed Central PMCID: 4312207].

[8] Zacharias WJ, Frank DB, Zepp JA, Morley MP, Alkhaleel FA, Kong J, et al. Regeneration of the lung alveolus by an evolutionarily conserved epithelial progenitor. Nature 2018 Mar 8;555(7695):251–5. PubMed PMID: 29489752.

[9] Giangreco A, Reynolds SD, Stripp BR. Terminal bronchioles harbor a unique airway stem cell population that localizes to the bronchoalveolar duct junction. Am J Pathol 2002 Jul;161(1):173–82 [PubMed PMID: 12107102. Pubmed Central PMCID: 1850682].

[10] Kim CF, Jackson EL, Woolfenden AE, Lawrence S, Babar I, Vogel S, et al. Identification of bronchioalveolar stem cells in normal lung and lung cancer. Cell 2005 Jun 17;121 (6):823–35 [PubMed PMID: 15960971].

[11] Nabhan AN, Brownfield DG, Harbury PB, Krasnow MA, Desai TJ. Single-cell Wnt signaling niches maintain stemness of alveolar type 2 cells. Science 2018 Mar 9;359 (6380):1118–23 [PubMed PMID: 29420258].

[12] Rock JR, Onaitis MW, Rawlins EL, Lu Y, Clark CP, Xue Y, et al. Basal cells as stem cells of the mouse trachea and human airway epithelium. Proc Natl Acad Sci U S A 2009 Aug 4;106(31):12771–5 [PubMed PMID: 19625615. Pubmed Central PMCID: 2714281].

[13] Hind M, Gilthorpe A, Stinchcombe S, Maden M. Retinoid induction of alveolar regeneration: from mice to man? Thorax 2009 May;64(5):451–7 [PubMed PMID: 19401491].

[14] Cunningham TJ, Duester G. Mechanisms of retinoic acid signalling and its roles in organ and limb development. Nat Rev Mol Cell Biol 2015 Feb;16(2):110–23 [PubMed PMID: 25560970. Pubmed Central PMCID: 4636111].

[15] Chen F, Cao Y, Qian J, Shao F, Niederreither K, Cardoso WV. A retinoic acid-dependent network in the foregut controls formation of the mouse lung primordium. J Clin Invest 2010 Jun;120(6):2040–8 [PubMed PMID: 20484817. Pubmed Central PMCID: 2877937].

[16] Malpel S, Mendelsohn C, Cardoso WV. Regulation of retinoic acid signaling during lung morphogenesis. Development 2000 Jul;127(14):3057–67 [PubMed PMID: 10862743].

[17] Massaro GD, Massaro D, Chambon P. Retinoic acid receptor-alpha regulates pulmonary alveolus formation in mice after, but not during, perinatal period. Am J Physiol Lung Cell Mol Physiol 2003 Feb;284(2):L431–3 [PubMed PMID: 12533315].

[18] Massaro GD, Massaro D, Chan WY, Clerch LB, Ghyselinck N, Chambon P, et al. Retinoic acid receptor-beta: an endogenous inhibitor of the perinatal formation of pulmonary alveoli. Physiol Genomics 2000 Nov 9;4(1):51–7 [PubMed PMID: 11074013].

[19] McGowan S, Jackson SK, Jenkins-Moore M, Dai HH, Chambon P, Snyder JM. Mice bearing deletions of retinoic acid receptors demonstrate reduced lung elastin and alveolar numbers. Am J Respir Cell Mol Biol 2000 Aug;23(2):162–7 [PubMed PMID: 10919981].

[20] Ng-Blichfeldt JP, Alcada J, Montero MA, Dean CH, Griesenbach U, Griffiths MJ, et al. Deficient retinoid-driven angiogenesis may contribute to failure of adult human lung regeneration in emphysema. Thorax 2017 Jun;72(6):510–21 [PubMed PMID: 28087752].

[21] Liu B, Harvey CS, McGowan SE. Retinoic acid increases elastin in neonatal rat lung fibroblast cultures. Am J Physiol 1993 Nov;265(5 Pt 1):L430–7 [PubMed PMID: 8238530].

[22] Checkley W, West Jr KP, Wise RA, Baldwin MR, Wu L, Leclerq SC, et al. Maternal vitamin A supplementation and lung function in offspring. N Engl J Med 2010 May 13; 362(19):1784–94 [PubMed PMID: 20463338].

[23] Soler Artigas M, Loth DW, Wain LV, Gharib SA, Obeidat M, Tang W, et al. Genome-wide association and large-scale follow up identifies 16 new loci influencing lung function. Nat Genet 2011 Sep 25;43(11):1082–90 [PubMed PMID: 21946350. Pubmed Central PMCID: 3267376].

[24] Plantier L, Rochette-Egly C, Goven D, Boutten A, Bonay M, Leseche G, et al. Dysregulation of elastin expression by fibroblasts in pulmonary emphysema: role of cellular retinoic acid binding protein 2. Thorax 2008 Nov;63(11):1012–7 [PubMed PMID: 18621984].

[25] Massaro GD, Massaro D. Retinoic acid treatment abrogates elastase-induced pulmonary emphysema in rats. Nat Med 1997 Jun;3(6):675–7 [PubMed PMID: 9176496].

[26] Hind M, Maden M. Retinoic acid induces alveolar regeneration in the adult mouse lung. Eur Respir J 2004 Jan;23(1):20–7 [PubMed PMID: 14738226].

[27] Belloni PN, Garvin L, Mao CP, Bailey-Healy I, Leaffer D. Effects of all-trans-retinoic acid in promoting alveolar repair. Chest 2000 May;117(5 Suppl 1) [235S–41S. PubMed PMID: 10843926].

[28] Tepper J, Pfeiffer J, Aldrich M, Tumas D, Kern J, Hoffman E, et al. Can retinoic acid ameliorate the physiologic and morphologic effects of elastase instillation in the rat? Chest 2000 May;117(5 Suppl 1) [242S–4eS. PubMed PMID: 10843928].

[29] Ishizawa K, Kubo H, Yamada M, Kobayashi S, Numasaki M, Ueda S, et al. Bone marrow-derived cells contribute to lung regeneration after elastase-induced pulmonary emphysema. FEBS Lett 2004 Jan 2;556(1–3):249–52 [PubMed PMID: 14706858].

[30] Stinchcombe SV, Maden M. Retinoic acid induced alveolar regeneration: critical differences in strain sensitivity. Am J Respir Cell Mol Biol 2008 Feb;38(2):185–91 [PubMed PMID: 17717321].

[31] Maden M. Retinoids have differing efficacies on alveolar regeneration in a dexamethasone-treated mouse. Am J Respir Cell Mol Biol 2006 Aug;35(2):260–7 [PubMed PMID: 16574940].

[32] Horiguchi M, Kojima H, Sakai H, Kubo H, Yamashita C. Pulmonary administration of integrin-nanoparticles regenerates collapsed alveoli. J Control Release 2014 Aug 10;187:167–74 [PubMed PMID: 24954410].

[33] Jones PW, Rames AD. Tesra (treatment of emphysema with a selective retinoid agonist) study results [abstract]. Am J Respir Crit Care Med 2011;183:A6418.

[34] Mao JT, Goldin JG, Dermand J, Ibrahim G, Brown MS, Emerick A, et al. A pilot study of all-trans-retinoic acid for the treatment of human emphysema. Am J Respir Crit Care Med 2002 Mar 01;165(5):718–23 [PubMed PMID: 11874821].

[35] Roth MD, Connett JE, D'Armiento JM, Foronjy RF, Friedman PJ, Goldin JG, et al. Feasibility of retinoids for the treatment of emphysema study. Chest 2006 Nov;130(5):1334–45 [PubMed PMID: 17099008].

[36] Stolk J, Stockley RA, Stoel BC, Cooper BG, Piitulainen E, Seersholm N, et al. Randomised controlled trial for emphysema with a selective agonist of the gamma-type retinoic acid receptor. Eur Respir J 2012 Aug;40(2):306–12 [PubMed PMID: 22282548].

[37] Barkauskas CE, Chung MI, Fioret B, Gao X, Katsura H, Hogan BL. Lung organoids: current uses and future promise. Development 2017 Mar 15;144(6):986–97 [PubMed PMID: 28292845. Pubmed Central PMCID: 5358104].

[38] Messier EM, Mason RJ, Kosmider B. Efficient and rapid isolation and purification of mouse alveolar type II epithelial cells. Exp Lung Res 2012 Sep;38(7):363–73 [PubMed PMID: 22888851].

[39] Yamada M, Kubo H, Ota C, Takahashi T, Tando Y, Suzuki T, et al. The increase of microRNA-21 during lung fibrosis and its contribution to epithelial-mesenchymal transition in pulmonary epithelial cells. Respir Res 2013 Sep 24;14:95 [PubMed PMID: 24063588. Pubmed Central PMCID: 3849377].

[40] McQualter JL, Yuen K, Williams B, Bertoncello I. Evidence of an epithelial stem/progenitor cell hierarchy in the adult mouse lung. Proc Natl Acad Sci U S A 2010 Jan 26;107(4):1414–9 [PubMed PMID: 20080639. Pubmed Central PMCID: 2824384].

[41] Teisanu RM, Chen H, Matsumoto K, McQualter JL, Potts E, Foster WM, et al. Functional analysis of two distinct bronchiolar progenitors during lung injury and repair. Am J Respir Cell Mol Biol 2011 Jun;44(6):794–803 [PubMed PMID: 20656948. Pubmed Central PMCID: 3135841].

[42] Ruijter JM, Ramakers C, Hoogaars WM, Karlen Y, Bakker O, van den Hoff MJ, et al. Amplification efficiency: linking baseline and bias in the analysis of quantitative PCR data. Nucleic Acids Res 2009 Apr;37(6):e45 [PubMed PMID: 19237396. Pubmed Central PMCID: 2665230].

[43] Ruijter JM, Pfaffl MW, Zhao S, Spiess AN, Boggy G, Blom J, et al. Evaluation of qPCR curve analysis methods for reliable biomarker discovery: bias, resolution, precision, and implications. Methods 2013 Jan;59(1):32–46 [PubMed PMID: 22975077].

[44] Kho AT, Liu K, Visner G, Martin T, Boudreault F. Identification of dedifferentiation and redevelopment phases during postpneumonectomy lung growth. Am J Physiol Lung Cell Mol Physiol 2013 Oct 15;305(8):L542–54 [PubMed PMID: 23997171. Pubmed Central PMCID: 3798774].

[45] Mendelsohn C, Ruberte E, Lemeur M, Morriss-Kay G, Chambon P. Developmental analysis of the retinoic acid-inducible RAR-beta 2 promoter in transgenic animals. Development 1991 Nov;113(3):723–34 [PubMed PMID: 1668276].

[46] Dong J, Feldmann G, Huang J, Wu S, Zhang N, Comerford SA, et al. Elucidation of a universal size-control mechanism in Drosophila and mammals. Cell 2007 Sep 21;130(6):1120–33 [PubMed PMID: 17889654. Pubmed Central PMCID: 2666353].

[47] Yu FX, Zhao B, Guan KL. Hippo pathway in organ size control, tissue homeostasis, and Cancer. Cell 2015 Nov 5;163(4):811–28 [PubMed PMID: 26544935. Pubmed Central PMCID: 4638384].

[48] Zanconato F, Forcato M, Battilana G, Azzolin L, Quaranta E, Bodega B, et al. Genome-wide association between YAP/TAZ/TEAD and AP-1 at enhancers drives oncogenic growth. Nat Cell Biol 2015 Sep;17(9):1218–27 [PubMed PMID: 26258633].

[49] Liu-Chittenden Y, Huang B, Shim JS, Chen Q, Lee SJ, Anders RA, et al. Genetic and pharmacological disruption of the TEAD-YAP complex suppresses the oncogenic activity of YAP. Genes Dev 2012 Jun 15;26(12):1300–5 [PubMed PMID: 22677547. Pubmed Central PMCID: 3387657].

[50] Volckaert T, Dill E, Campbell A, Tiozzo C, Majka S, Bellusci S, et al. Parabronchial smooth muscle constitutes an airway epithelial stem cell niche in the mouse lung after injury. J Clin Invest 2011 Nov;121(11):4409–19 [PubMed PMID: 21985786. Pubmed Central PMCID: 3204843].

[51] Yanagita K, Matsumoto K, Sekiguchi K, Ishibashi H, Niho Y, Nakamura T. Hepatocyte growth factor may act as a pulmotrophic factor on lung regeneration after acute lung injury. J Biol Chem 1993 Oct 5;268(28):21212–7 [PubMed PMID: 8407957].

[52] Panos RJ, Patel R, Bak PM. Intratracheal administration of hepatocyte growth factor/scatter factor stimulates rat alveolar type II cell proliferation in vivo. Am J Respir Cell Mol Biol 1996 Nov;15(5):574–81 [PubMed PMID: 8918364].

[53] Yildirim AO, Muyal V, John G, Muller B, Seifart C, Kasper M, et al. Palifermin induces alveolar maintenance programs in emphysematous mice. Am J Respir Crit Care Med 2010 Apr 1;181(7):705–17 [PubMed PMID: 20007933].

[54] Lu J, Izvolsky KI, Qian J, Cardoso WV. Identification of FGF10 targets in the embryonic lung epithelium during bud morphogenesis. J Biol Chem 2005 Feb 11;280(6):4834–41 [PubMed PMID: 15556938].

[55] Germain P, Gaudon C, Pogenberg V, Sanglier S, Van Dorsselaer A, Royer CA, et al. Differential action on coregulator interaction defines inverse retinoid agonists and neutral antagonists. Chem Biol 2009 May 29;16(5):479–89 [PubMed PMID: 19477412].

[56] Lee JH, Bhang DH, Beede A, Huang TL, Stripp BR, Bloch KD, et al. Lung stem cell differentiation in mice directed by endothelial cells via a BMP4-NFATc1-thrombospondin-1 axis. Cell 2014 Jan 30;156(3):440–55 [PubMed PMID: 24485453. Pubmed Central PMCID: 3951122].

[57] Zhang Y, Zolfaghari R, Ross AC. Multiple retinoic acid response elements cooperate to enhance the inducibility of CYP26A1 gene expression in liver. Gene 2010 Sep 15;464(1–2):32–43 [PubMed PMID: 20682464. Pubmed Central PMCID: 2916872].

[58] Lee LM, Leung CY, Tang WW, Choi HL, Leung YC, McCaffery PJ, et al. A paradoxical teratogenic mechanism for retinoic acid. Proc Natl Acad Sci U S A 2012 Aug 21;109(34):13668–73 [PubMed PMID: 22869719. Pubmed Central PMCID: 3427051].

[59] Niederreither K, Subbarayan V, Dolle P, Chambon P. Embryonic retinoic acid synthesis is essential for early mouse post-implantation development. Nat Genet 1999 Apr;21(4):444–8 [PubMed PMID: 10192400].

[60] Mendelsohn C, Lohnes D, Decimo D, Lufkin T, Lemeur M, Chambon P, et al. Function of the retinoic acid receptors (RARs) during development (II). Multiple abnormalities at various stages of organogenesis in RAR double mutants. Development 1994 Oct;120(10):2749–71 [PubMed PMID: 7607068].

[61] Weber E, Ravi RK, Knudsen ES, Williams JR, Dillehay LE, Nelkin BD, et al. Retinoic acid-mediated growth inhibition of small cell lung cancer cells is associated with reduced myc and increased p27Kip1 expression. Int J Cancer 1999 Mar 15;80(6):935–43 [PubMed PMID: 10074929].

[62] Langenfeld J, Kiyokawa H, Sekula D, Boyle J, Dmitrovsky E. Posttranslational regulation of cyclin D1 by retinoic acid: a chemoprevention mechanism. Proceedings of the National Academy of Sciences of the United States of America. 1997 Oct 28;vol. 94 (22):[12070–4. PubMed PMID: 9342364. Pubmed Central PMCID: 23705].

[63] Noy N. Between death and survival: retinoic acid in regulation of apoptosis. Annu Rev Nutr 2010 Aug 21;30:201–17 [PubMed PMID: 20415582].

[64] Berard J, Laboune F, Mukuna M, Masse S, Kothary R, Bradley WE. Lung tumors in mice expressing an antisense RARbeta2 transgene. FASEB J 1996 Jul;10(9):1091–7 [PubMed PMID: 8801172].

[65] Houle B, Rochette-Egly C, Bradley WE. Tumor-suppressive effect of the retinoic acid receptor beta in human epidermoid lung cancer cells. Proceedings of the National Academy of Sciences of the United States of America. 1993 Feb 1;vol. 90(3):[985–9. PubMed PMID: 8381540. Pubmed Central PMCID: 45795].

[66] Xu XC, Sozzi G, Lee JS, Lee JJ, Pastorino U, Pilotti S, et al. Suppression of retinoic acid receptor beta in non-small-cell lung cancer in vivo: implications for lung cancer development. J Natl Cancer Inst 1997 May 7;89(9):624–9 [PubMed PMID: 9150186].

[67] Gebert JF, Moghal N, Frangioni JV, Sugarbaker DJ, Neel BG. High frequency of retinoic acid receptor beta abnormalities in human lung cancer. Oncogene 1991 Oct;6(10):1859–68 [PubMed PMID: 1717924].

[68] Boyd JM, Gallo GJ, Elangovan B, Houghton AB, Malstrom S, Avery BJ, et al. Bik, a novel death-inducing protein shares a distinct sequence motif with Bcl-2 family proteins and interacts with viral and cellular survival-promoting proteins. Oncogene 1995 Nov 2;11(9):1921–8 [PubMed PMID: 7478623].

[69] Yang L, Zhao H, Li SW, Ahrens K, Collins C, Eckenrode S, et al. Gene expression profiling during all-trans retinoic acid-induced cell differentiation of acute promyelocytic leukemia cells. J Mol Diagn 2003 Nov;5(4):212–21 [PubMed PMID: 14573779. Pubmed Central PMCID: 1907337].

[70] Liu Z, Wu H, Jiang K, Wang Y, Zhang W, Chu Q, et al. MAPK-Mediated YAP activation controls mechanical-tension-induced pulmonary alveolar regeneration. Cell Rep 2016 Aug 16;16(7):1810–9 [PubMed PMID: 27498861].

[71] Mahoney JE, Mori M, Szymaniak AD, Varelas X, Cardoso WV. The hippo pathway effector Yap controls patterning and differentiation of airway epithelial progenitors. Dev Cell 2014 Jul 28;30(2):137–50 [PubMed PMID: 25043473].

[72] Zhao R, Fallon TR, Saladi SV, Pardo-Saganta A, Villoria J, Mou H, et al. Yap tunes airway epithelial size and architecture by regulating the identity, maintenance, and self-renewal of stem cells. Dev Cell 2014 Jul 28;30(2):151–65 [PubMed PMID: 25043474. Pubmed Central PMCID: 4130488].

[73] Lange AW, Sridharan A, Xu Y, Stripp BR, Perl AK, Whitsett JA. Hippo/Yap signaling controls epithelial progenitor cell proliferation and differentiation in the embryonic and adult lung. J Mol Cell Biol 2015 Feb;7(1):35–47 [PubMed PMID: 25480985. Pubmed Central PMCID: 4400400].

[74] Zanconato F, Cordenonsi M, Piccolo S. YAP/TAZ at the Roots of Cancer. Cancer Cell 2016 Jun 13;29(6):783–803 [PubMed PMID: 27300434].

[75] Lau AN, Curtis SJ, Fillmore CM, Rowbotham SP, Mohseni M, Wagner DE, et al. Tumor-propagating cells and Yap/Taz activity contribute to lung tumor progression and metastasis. EMBO J 2014 Mar 3;33(5):468–81 [PubMed PMID: 24497554. Pubmed Central PMCID: 3989628].

[76] Zhang W, Gao Y, Li F, Tong X, Ren Y, Han X, et al. YAP promotes malignant progression of Lkb1-deficient lung adenocarcinoma through downstream regulation of survivin. Cancer Res 2015 Nov 1;75(21):4450–7 [PubMed PMID: 26363011].

[77] Rizvi S, Yamada D, Hirsova P, Bronk SF, Werneburg NW, Krishnan A, et al. A Hippo and Fibroblast Growth factor Receptor Autocrine Pathway in Cholangiocarcinoma. J Biol Chem 2016 Apr 8;291(15):8031–47 [PubMed PMID: 26826125. Pubmed Central PMCID: 4825008].

[78] Hansen CG, Moroishi T, Guan KL. YAP and TAZ: a nexus for Hippo signaling and beyond. Trends Cell Biol 2015 Sep;25(9):499–513 [PubMed PMID: 26045258. Pubmed Central PMCID: 4554827].

[79] Schuldiner M, Yanuka O, Itskovitz-Eldor J, Melton DA, Benvenisty N. Effects of eight growth factors on the differentiation of cells derived from human embryonic stem cells. Proceedings of the National Academy of Sciences of the United States of America. 2000 Oct 10;vol. 97(21):[11307–12. PubMed PMID: 11027332. Pubmed Central PMCID: 17196].

[80] Okada Y, Shimazaki T, Sobue G, Okano H. Retinoic-acid-concentration-dependent acquisition of neural cell identity during in vitro differentiation of mouse embryonic stem cells. Dev Biol 2004 Nov 1;275(1):124–42 [PubMed PMID: 15464577].

[81] Lasagni L, Angelotti ML, Ronconi E, Lombardi D, Nardi S, Peired A, et al. Podocyte regeneration driven by renal progenitors determines glomerular disease remission and can be pharmacologically enhanced. Stem Cell Rep 2015 Aug 11;5(2):248–63 [PubMed PMID: 26235895. Pubmed Central PMCID: 4618832].

[82] Peired A, Angelotti ML, Ronconi E, la Marca G, Mazzinghi B, Sisti A, et al. Proteinuria impairs podocyte regeneration by sequestering retinoic acid. J Am Soc Nephrol 2013 Nov;24(11):1756–68 [PubMed PMID: 23949798. Pubmed Central PMCID: 3810076].

[83] Jacobs S, Lie DC, Decicco KL, Shi Y, Deluca LM, Gage FH, et al. Retinoic acid is required early during adult neurogenesis in the dentate gyrus. Proc Natl Acad Sci U S A 2006 Mar 7;103(10):3902–7 [PubMed PMID: 16505366. Pubmed Central PMCID: 1450163].

[84] Gray TE, Guzman K, Davis CW, Abdullah LH, Nettesheim P. Mucociliary differentiation of serially passaged normal human tracheobronchial epithelial cells. Am J Respir Cell Mol Biol 1996 Jan;14(1):104–12 [PubMed PMID: 8534481].

[85] Clamon GH, Sporn MB, Smith JM, Saffiotti U. Alpha- and beta-retinyl acetate reverse metaplasias of vitamin a deficiency in hamster trachea in organ culture. Nature 1974 Jul 5;250(461):64–6 [PubMed PMID: 4841587].

[86] Wolbach SB, Howe PR. Epithelial repair in recovery from vitamin a deficiency : an experimental study. J Exp Med 1933 Feb 28;57(3):511–26 [PubMed PMID: 19870144. Pubmed Central PMCID: 2132241].

[87] Hahn CK, Ross KN, Warrington IM, Mazitschek R, Kanegai CM, Wright RD, et al. Expression-based screening identifies the combination of histone deacetylase inhibitors and retinoids for neuroblastoma differentiation. Proc Natl Acad Sci U S A 2008 Jul 15;105(28):9751–6 [PubMed PMID: 18607002. Pubmed Central PMCID: 2474517].

[88] Pili R, Salumbides B, Zhao M, Altiok S, Qian D, Zwiebel J, et al. Phase I study of the histone deacetylase inhibitor entinostat in combination with 13-cis retinoic acid in patients with solid tumours. Br J Cancer 2012 Jan 3;106(1):77–84 [PubMed PMID: 22134508. Pubmed Central PMCID: 3251867].

[89] Soriano AO, Yang H, Faderl S, Estrov Z, Giles F, Ravandi F, et al. Safety and clinical activity of the combination of 5-azacytidine, valproic acid, and all-trans retinoic acid in acute myeloid leukemia and myelodysplastic syndrome. Blood 2007 Oct 1;110(7):2302–8 [PubMed PMID: 17596541].

[90] Gudas LJ, Wagner JA. Retinoids regulate stem cell differentiation. J Cell Physiol 2011 Feb;226(2):322–30 [PubMed PMID: 20836077. Pubmed Central PMCID: 3315372].

[91] Schmidt CK, Brouwer A, Nau H. Chromatographic analysis of endogenous retinoids in tissues and serum. Anal Biochem 2003 Apr 1;315(1):36–48 [PubMed PMID: 12672410].

[92] Guo X, Ruiz A, Rando RR, Bok D, Gudas LJ. Esterification of all-trans-retinol in normal human epithelial cell strains and carcinoma lines from oral cavity, skin and breast: reduced expression of lecithin:retinol acyltransferase in carcinoma lines. Carcinogenesis 2000 Nov;21(11):1925–33 [PubMed PMID: 11062150].

[93] Wright JL, Cosio M, Churg A. Animal models of chronic obstructive pulmonary disease. Am J Physiol Lung Cell Mol Physiol 2008 Jul;295(1):L1–15 [PubMed PMID: 18456796. Pubmed Central PMCID: 2494776].